



HORIZON 2020

THEME SC5-2017



European Climate Prediction system

(Grant Agreement 776613)

**European Climate Prediction system (EUCP)**

**Deliverable D3.4**

***Portfolio of suitable post-processed high-impact weather events for the present day and near future***

Deliverable Title	<i>Portfolio of suitable post-processed high-impact weather events for the present day and near future</i>	
Brief Description	<i>We report on WP3 data delivered to WP4 for their impact studies and provide a description of selected high impact weather events as simulated by the CPMs for the various domains.</i>	
WP number	3	
Lead Beneficiary	<i>Thomas Frisius (GERICS)</i>	
Contributors	<i>Danijel Belušić (SMHI), Petter Lind (SMHI), Marianna Adinolfi (CMCC), Paola Mercogliano (CMCC), Mario Raffa (CMCC), Namendra Kumar-Shahi (IPSL), Jan Polcher (IPSL), Sophie Bastin (IPSL), Ségolène Berthou (UKMO), Ole B. Christensen (DMI), Hylke de Vries (KNMI), Thomas Frisius (GERICS), Emanuela Picheli (ICTP), Cécile Caillaud (CNRS-CNRM), Erwan Brisson (CNRS-CNRM), Antoinette Alias (CNRS-CNRM), Quentin Fumière (CNRS-CNRM), Samuel Somot (CNRS-CNRM), Albrecht Weerts (Deltares), Marjanne Zander (Deltares)</i>	
Creation Date	<i>01/02/2022</i>	
Version Number	<i>3.0</i>	
Version Date	<i>01/03/2022</i>	
Deliverable Due Date	<i>31/03/2022</i>	
Actual Delivery Date	<i>31/05/2022</i>	
Nature of the Deliverable	<input checked="" type="checkbox"/>	<i>R – Report</i>
	<input type="checkbox"/>	<i>P - Prototype</i>
	<input type="checkbox"/>	<i>D - Demonstrator</i>
	<input type="checkbox"/>	<i>O - Other</i>
Dissemination Level/ Audience	<input type="checkbox"/>	<i>PU - Public</i>
	<input checked="" type="checkbox"/>	<i>PP - Restricted to other programme participants, including the Commission services</i>
	<input type="checkbox"/>	<i>RE - Restricted to a group specified by the consortium, including the Commission services</i>
	<input type="checkbox"/>	<i>CO - Confidential, only for members of the consortium, including the Commission services</i>

Version	Date	Modified by	Comments
0.0	01/02/2022	Thomas Frisius	Created
1.0	01/03/2022	Thomas Frisius	First draft
2.0	31/03/2022	Thomas Frisius	Version submitted to coordination team
3.0	30/05/2022	Thomas Frisius	Updated based on coordination team comments – Final version

## **Table of contents**

1. Executive Summary.....	6
2. Project Objectives.....	6
3. Detailed Report.....	6
3.1 Introduction.....	6
3.2 Data delivered to WP4.....	7
3.2.1 Available CPM data fields.....	7
3.2.2 Alpine flash floods.....	9
3.2.3 Compound flood analysis on Caribbean Islands (e.g. Martinique, St Martin, Guadeloupe).....	9
3.2.4 Changes in drought and river flooding on La Réunion.....	10
3.3 Analysis of selected high impact weather events in various CPM domains .....	11
3.3.1 NWE-3: Winter storms.....	12
3.3.1.1 Wind changes in NWE-3 domain (single model analysis).....	12
3.3.1.2 Precipitation changes in NWE-3 domain (multi-model analysis).....	15
3.3.2 CEU-3: Continuous Heavy rain.....	19
3.3.3 SWE-3: Droughts.....	22
3.3.4 ALP-3: Fall Mediterranean heavy precipitation events.....	25
3.3.4.1 Aim of the study.....	25
3.3.4.2 Methodology .....	25
3.3.4.3 HPEs spatial density.....	26
3.3.4.4 HPEs characteristics over French Mediterranean Area .....	27
3.3.4.5 Conclusion .....	30
3.3.5 NEU-3: Polar lows.....	30
4. Lessons Learnt and links built.....	33
5. References.....	33

### List of Tables

Table 1: Core variables provided by WP3 .....	8
Table 2: Additional variables provided by WP3 for some simulations .....	8
Table 3: Metrics on CDD index over Spain (common domain) for the evaluation experiment (2000-2009).....	23
Table 4: Metrics on CDD index over SW-3 domain for the historical experiment (1996-2005).....	23
Table 5: Metrics on CDD index over SW-3 domain for the near future experiment (2041-2050).....	24
Table 6: Modelling systems used by the participating groups.....	26

### List of Figures

Figure 1. Observed and simulated precipitation for the current La Réunion climate (2000-2010).....	10
Figure 2. Observed and simulated precipitation for current and future La Réunion climate.....	11
Figure 3. Observed and corrected simulated precipitation for current and future La Réunion climate.....	11
Figure 4: Set of domains used for CPM simulations. In addition to the sub-continental domains covered	

by the modelling groups, the dashed box indicates the Reduced Europe domain (REU-3) used by ETHZ and UKMO..... 12

Figure 5: Time series of power dissipation index deduced from the a) historical run (1996-2005), b) near future run (2041-2050) and c) End of Century run (2090-2099) for the NWE-3 domain..... 13

Figure 6: Selected snap-shots of the NWE-3 simulation displaying 10m wind speed (coloured shadings, m/s) and sea level pressure (hPa). These figures show the passage of a very intense winter storm..... 14

Figure 7: a) Time-averaged power dissipation index for the various simulations and its climate change, b) frequency distribution of the power dissipation index for the various simulations..... 14

Figure 8: Percentage change in mean winter precipitation at the end of the century compared to the reference period. Left: convection-parameterised RCM, Right: convection-permitting models. The box shows where extratropical cyclone tracks are selected..... 16

Figure 9: Examples of storms selected for each model: two different storms (left/right) in the CPM (top) or RCM (bottom). Storm sector definitions are explained in the legend, frontal zones are defined as areas with the norm of Wet Bulb Potential Temperature gradients stronger than 4K/110km (or 5km/110km for MOHC model on a 25km grid)..... 17

Figure 10: Precipitation contribution to the mean within storms (frequency x value of bin, using exponential bins defined in Berthou et al. (2019)). This way, the area under the curve is mean precipitation for the present-day (thin lines) and end-of-century mean precipitation increase (future-present, thick lines). Contribution from all points in storms (black), points in warm sector (red), cold sector (blue), central sector (purple) and strong WPBT gradients (grey), as defined in Fig.5. Plain line is for CPM, dashed line for RCM..... 18

Figure 11: Density of 850hPa Wet bulb temperature (black line with grey shading, left axis). Occurrence of low (0.1 to 1mm/h) and moderate (1 to 5mm/h) precipitation scaled by 1/10; intense (5-10mm/h) and heavy (>10mm/h) precipitation; CAPE (>250J/kg) and CIN (<-100J/kg), both scaled by 1/10, all binned by WPBT values and normalised by the number of points in all storms, on the native grid in the MOHC CPM. a) present-day winter storms, b) future end-of-century winter storms and c) present-day autumn storms..... 19

Figure 12: Time series of precipitated water mass deduced from the a) historical run (1996-2005) and b) near future run (2041-2050) for the CEU-3 domain..... 20

Figure 13: Selected snap-shots of the CEU-3 simulation displaying accumulated precipitation (mm) of consecutive days and sea level pressure (hPa). These figures show a continuous heavy rain case with high precipitated water mass.....21

Figure 14: Scatter diagram: precipitated water mass versus area for the two CEU-3 simulations.... 21

Figure 15: Consecutive dry days index for the period 2000-2009 over SW3 domain..... 23

Figure 16: Comparison between historical period and near future for consecutive dry days index over SWE-3 domain..... 24

Figure 17: Box plots for consecutive dry days in historical experiment and near future from CPM results..... 24

Figure 18: CNRM-AROME topography for the pan-Alpine domain. Delimited by black lines, the regular ALP3 domain is used as the tracking domain and the French Med area is delimited by black dotted lines..... 27

Figure 19: Spatial density of cells above 10mm/h (number per year) during extended fall (SOND) for the historical period (1996-2005) for the 9 CPMs (driving GCMs are given under the model name), the multi-model ensemble and the observations (2000-2009, available only over lands of France, Italy,

Switzerland and Germany)..... 28

Figure 20: Raw differences of spatial density of cells (number per year) above 10mm/h during extended fall (SOND) between the mid century period (2041-2050) and the historical period (1996-2005) for the 9 CPMs and the multi-model ensemble. The number of models in tendency agreement is also given, considering only changes in number of cells above two..... 28

Figure 21: Intensity duration frequency (IDF) plot considering all tracks of cells above 10 mm/h occurring during days exceeding 100 mm/day in the French MED area during the extended fall (SOND) for the historical period (1996-2005) for the 9 CPMs (the number of tracks is given for each model), the multi-model ensemble and observations (1997-2016)..... 29

Figure 22: Differences of intensity duration frequency (IDF) plot considering all tracks of cells above 10 mm/h occurring during days exceeding 100 mm/day in the French MED area during the extended fall (SOND) between the mid century period (RCP85 2041-2050) and the historical period (1996-2005) for the 9 CPMs (the evolution of the number of tracks is given for each model) and the multi-model ensemble. The number of models in tendency agreement is also given, considering only changes in frequency above 0.15%..... 29

Figure 23: Identified polar low tracks in the historical (left panel) and near future (right panel) simulations..... 31

Figure 24: Time series of polar low counts for the historical (left panel) and near future (right panel) simulations..... 31

Figure 25: Selected snap-shots of the NEU-3 simulation displaying an intense polar low case (contours: sea level pressure, shadings: precipitation (mm/hr), 10m wind (coloured wind barbs, kts)..... 32

Figure 26: Frequency distribution of maximum 10m wind speed in the polar low identified in the NEU-3 simulations..... 33

## **1. Executive summary**

We present deliverable 3.4 of the Work Package 3 (WP3): “Demonstrator of high impact weather in a changing climate on regional and local scales”. This deliverable informs about a portfolio of high impact extreme meteorological events at the pan-European level using convection-permitting regional climate models (CPMs) running at horizontal grid spacings of 2.2-3 km.

The report contains descriptions of i) postprocessed datasets that were made available on two data servers, ii) use of the data in Work Package 4 (WP4) impact studies and iii) a set of manifold high impact weather events which were analysed for the various pan-European model domains. It can be demonstrated that the comprehensive multi-model multi-domain CPM ensemble provides a great benefit for examining high impact weather events in a changing climate on regional and local scales.

## **2. Project objectives**

These deliverables have contributed to the following EUCP objectives (Description of Action, Section 1.1):

No.	Objective	Yes	No
1	Develop an ensemble climate prediction system based on high-resolution climate models for the European region for the near-term (~1-40 years)	✓	
2	Use the climate prediction system to produce consistent, authoritative and actionable climate information	✓	
3	Demonstrate the value of this climate prediction system through high impact extreme weather events in the near past and near future	✓	
4	Develop, and publish, methodologies, good practice and guidance for producing and using EUCP’s authoritative climate predictions for 1-40 year timescales	✓	

## **3. Detailed report**

### **3.1 Introduction**

Deliverable 3.4 contributes further analysis to WP3. It is split in two parts. The first part describes the sharing of the CMORized data of the convection permitting model (CPM) ensemble (see also report for deliverable 3.3) with WP4. In the second part the analysis of some exemplary high impact weather events for the various model domains (listed in report for deliverable 3.1) are presented.

## **3.2 Data delivered to WP4**

The output of convection permitting models forms a suitable input for smaller scale weather impact models. First, we describe which CMORized data have been made available to WP4 and other users. Afterwards, we provide more details about the WP4 impact studies using WP3 data.

### **3.2.1 Available CPM data fields**

For every model domain (see Fig. 1. in report on deliverable 3.3), every model in the ensemble (see table 1 in report on deliverable 3.3) the core variables listed in table 1 were provided. These were generated for the Evaluation runs (ERA-Interim driven, 1/1/2000 - 31/12/2009), Historical runs (GCM-driven, 1/1/1996 - 31/12/2005), Near future runs (GCM-driven, RCP8.5, 1/1/2041 - 31/12/2050) and, when available, the end of century runs (GCM, RCP8.5, 1/1/2090 - 31/12/2099). The results of intermediate forcing RCMs (see table 1 in report on deliverable 3.3) were also uploaded in addition to the CPM data. Additional optional variables listed in table 2 were also provided for some simulations. Data for the pan-Alpine domain ALP-3 are stored on the Juelich-Server jsc-cordex.fz-juelich.de within the framework of the CORDEX FPS-Convection project while the data for the other domains have been uploaded to the DMI EUCP-server eucp@ensemblesrt3.dmi.dk.

The naming convention of the CMORized files is as follows

<var>\_<domain>\_<gcm>\_<run>\_<model>\_<member>\_<rcm\_version\_id>\_<freq>\_<start>-<end>.nc

where

<var> Variable (abbreviation, see table 1 and 2)

<domain> Name of model domain

<gcm> Name of forcing GCM

<run> Name of the simulation

<model> Name of the model

<member> Driving model ensemble member (usually r1i1p1)

<rcm\_version\_id> ID of RCM version

<freq> Temporal frequency

<start> Time of the first record in the file

<end> Time of the last record in the file

An example file name is given by

pr\_NWE-3\_CNRM-CERFACS-CNRM-CM5\_rcp85\_r1i1p1\_CNRM-AROME41t1\_fpsconv-x2yn2-v1\_1hr\_204101010030-204112312330.nc

On the server jsc-cordex.fz-juelich.de the data are stored in the directory

/mnt/CORDEX\_FPS\_CPCM/CORDEX-FPSCONV/output

and on the eucp@ensemblesrt3.dmi.dk server it is

/archive/EUCP/output

The sub-directories are named as follows

<domain>/<institute>/<gcm>/<run>/<member>/<model>/<rcm\_version\_id>/<freq>/<var>

where <institute> names the institute that conducted the run. An example for a sub-directory is

NWE-3/CNRM/CNRM-CERFACS-CNRM-CM5/historical/r1i1p1/CNRM-AROME41t1/fpsconv-x2yn2-v1/1hr/pr

The investigators of WP4 also utilize WP3 data based on Outer-European domain simulations for the Caribbean and La Réunion. The data produced by these simulations will be described in the report for deliverable 3.5.

*Table 1: Core variables provided by WP3.*

Variable	Abbreviation	Temporal frequency	Unit
Precipitation	pr	hourly	kg m <sup>-2</sup> s <sup>-1</sup>
Solid part of precipitation	prsolid	hourly	kg m <sup>-2</sup> s <sup>-1</sup>
Near-surface air temperature	tas	hourly	K
Sea level pressure	psl	hourly	Pa
Near-surface specific humidity	huss	hourly	1
Surface downwelling shortwave radiation	rsds	hourly	Wm <sup>-2</sup>
Total cloud fraction	clt	hourly	%
Eastward near-surface wind	uas	hourly	m s <sup>-1</sup>
Northward near-surface wind	vas	hourly	m s <sup>-1</sup>

*Table 2: Additional variables provided by WP3 for some simulations.*

Variable	Abbreviation	Temporal frequency	Unit
Daily maximum Near-surface air temperature	tasmax	daily	K
Daily minimum Near-surface air temperature	tasmin	daily	K
Near-surface relative humidity	hurs	highest	%
Surface upward latent heat flux	hfls	highest	Wm <sup>-2</sup>
Surface upward sensible heat flux	hfss	highest	Wm <sup>-2</sup>
Surface downwelling longwave radiation	rlds	highest	Wm <sup>-2</sup>

Specific humidity 850hPa	hus850	highest	1
Specific humidity 500hPa	hus500	highest	1
Specific humidity 200hPa	hus200	highest	m s <sup>-1</sup>
Air temperature 850hPa	ta850	highest	K
Air temperature 500hPa	ta500	highest	K
Air temperature 200hPa	ta200	highest	K

### **3.2.2 Alpine flash floods**

The precipitation fields, as well as temperature, surface pressure, and incoming shortwave radiation fields of the ALP-3 domain CPM simulations with hourly sampling frequency were used by Deltares to drive the high-resolution distributed hydrological model wflow-sbm (Imhoff et al. 2020) for the i) evaluation period, ii) historical period and iii) end of century period. The results are utilized to investigate flash-floods at several locations in the Alpine region. Two papers on this study are in preparation (preliminary results were presented by Zander et al. 2021).

For this study a subsample of the ensemble is chosen comprising the CMCC, CNRS-CNRM, ETHZ, ICTP, KNMI, SMHI, and UKMO simulations. The simulations of the evaluation period / ERA-Interim simulations (2000-2012) are used to compare the performance of the combination of climate model and hydrological model, and to assess the ability of the models to reproduce recorded flash floods.

Preliminary investigations reveal that direct ERA-5 driven validation simulations generally clearly outperform the evaluation simulation based on the ERA-Interim driven CPM UM (UKMO CPM) when comparing with discharge peaks at stations. This indicates that the CP-RCM downscaled ERA-Interim precipitation is not as good as the more recently released ERA5 data. Future simulations indicate for the considered locations in the Alpine region a decrease in flash flood number but that the flash flood will become more devastating.

### **3.2.3 Compound flood analysis on Caribbean Islands (e.g. Martinique, St Martin, Guadeloupe)**

For assessment of climate change impact on compound flooding in the Caribbean by Deltares the 2D inundation modelling model SFINCS (Leijnse et al. 2021) is used. SFINCS obtains the sea boundary conditions from Global Tide and Surge Model (GTSM) simulations (Delft3D FM, Deltares 2019) driven by the pseudo global warming (PGW) simulations from KNMI (more details will appear in the report on deliverable 3.5). Currently, sea level rise is added as postprocessing to those GTSM simulations but could also be incorporated in the Delft3D FM GTSM model. The river boundary conditions are provided by wflow\_sbm models setup for the Caribbean Islands which are driven by the rainfall and potential evaporation forcing from the KNMI PGW CPM runs. As the PGW runs are only available for part of the year CHIRPS rainfall data (Funk et al. 2015) and ERA5 are used to derive plausible initial conditions for the hydrological model depending on the time of year. The length of the PGW runs ensures that those initial conditions do not play a role in the inundation calculations.

A first step in the analysis is to look at the impact of the PGW on the calculated water level. The second step is to calculate the impact of historical events (inc damages using Delft FIAT).

### 3.2.4 Changes in drought and river flooding on La Réunion

The current and future climate simulation runs for La Réunion provided by CNRS-CNRM were used by Deltares to drive the hydrological model wflow-sbm in order to investigate changes in drought and river flooding. A first check was made to check the frequency of rainfall to see if a wet/dry day correction was needed. Figure 1 shows that the observed and simulated frequency distributions of daily precipitation are similar and no correction (e.g. a threshold) was applied. A daily observation dataset (1979-2019) for La Reunion has been used that was provided by Meteo-France for the EUCP project.

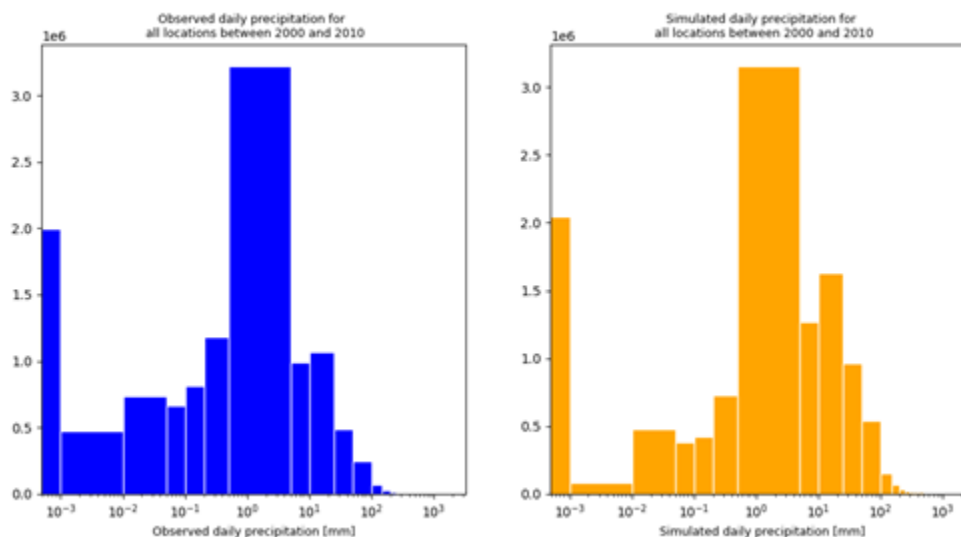


Figure 1. Observed and simulated precipitation for the current La Réunion climate (2000-2010).

A second step was to check the simulated annual cycle of precipitation against observations. Figure 2 is showing that the amount of rainfall is somewhat too high and there it was decided to perform a simple linear scaling bias correction on a monthly basis as shown in Figure 3. Finally, the corrected current and future climate model forcing was used to drive the hydrological wflow\_sbm model developed for La Reunion within EUCP.

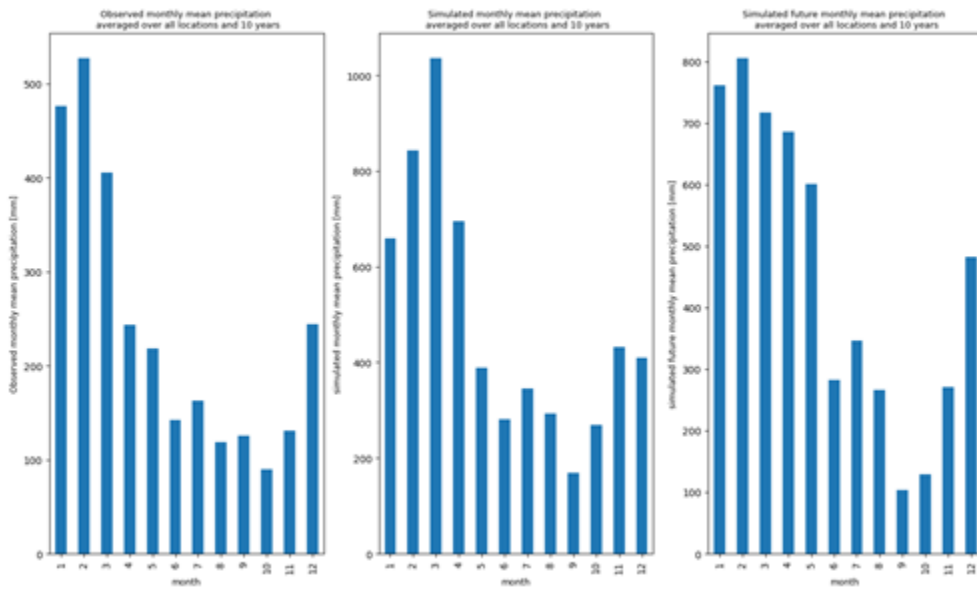


Figure 2. Observed and simulated precipitation for current and future La Réunion climate (note the different ordinate scales).

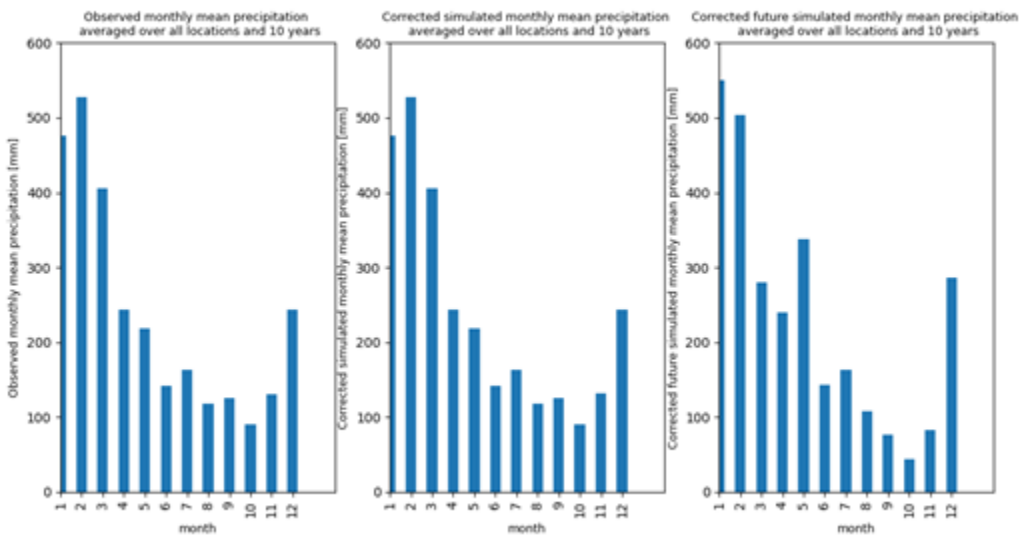


Figure 3. Observed and corrected simulated precipitation for current and future La Réunion climate.

### **3.3 Analysis of selected high impact weather events in various CPM domains**

A set of exemplary high impact weather event analysis for the historical and future periods is presented in this section. One characteristic event is analysed for each model domain (see Fig. 4). These are winter storms (NWE-3), continuous heavy rain (CEU-3), droughts (SWE-3), fall Mediterranean heavy precipitation (ALP-3) and polar lows (NEU-3). The analysis of hourly extreme precipitation in the SEE-3 and CEE-3 domains was already described in the report for deliverable 3.3.

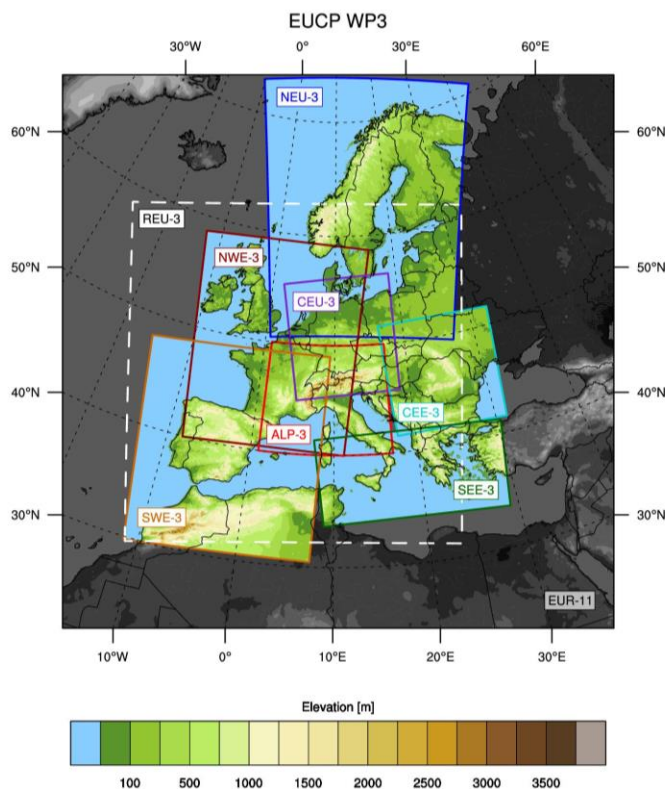


Figure 4. Set of domains used for CPM simulations. In addition to the sub-continental domains covered by the modelling groups, the dashed box indicates the Reduced Europe domain (REU-3) used by ETHZ and UKMO.

### **3.3.1 NWE-3: Winter storms**

#### **3.3.1.1 Wind changes in NWE-3 domain (single model analysis)**

For the evaluation of winter storms we select the NWE-3 simulations executed by CNRM with the CPM CNRM-AROME. To detect winter storms we applied the following analysis method:

- The number of consecutive hours with more than 5m/s wind speed at 10m overland are calculated.
- The power dissipation<sup>1</sup> (=cube of wind speed) of the period with consecutive 5m/s wind speed hours is determined.
- The power dissipation values of those grid-points which have at least 3 consecutive hours of wind speed with more than 5m/s and an actual wind speed of more than 15m/s are added.

Fig. 5 shows the time series of this index for the historical, near future and end of century period. As expected, this index indicates more storm activity in winter. There is also visible interannual variability, i.e., some winters have events with a very high index (e.g. winter 2003/04) while in other winters the index does not reach outstanding values (e.g. winter 1997/98). We recall that years indicated here do not correspond to real years. It is indicated that the index becomes higher in the near future while this is less obvious at the end of the century.

<sup>1</sup> Emanuel (2005) introduced a power dissipation index for tropical cyclones. It serves as an indicator for the potential destructiveness of these storms. Here, we apply this idea to winter storms.

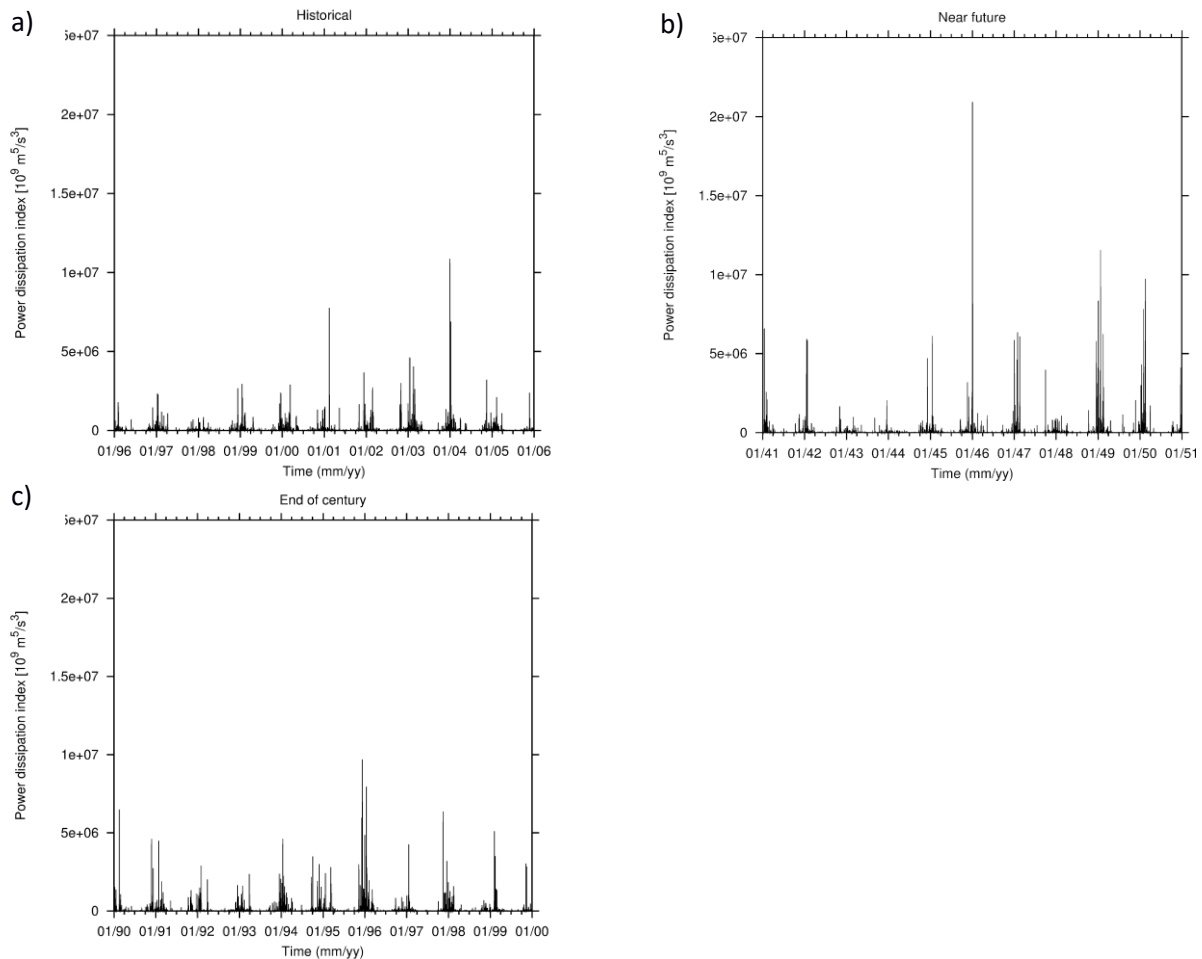


Figure 5: Time series of power dissipation index deduced from the a) historical run (1996-2005), b) near future run (2041-2050) and c) end of century run (2090-2099) for the NWE-3 domain.

Fig. 6 shows an outstanding example for a winter storm. It is associated with the peak of the power dissipation index in winter 2003/04 (Fig. 5a). This is a typical west weather situation in which an eastward moving cyclone is embedded in a westerly zonal flow. In this case the highest wind speeds are observed in the southern sector of the cyclone. This storm brings strong winds to France, Southern England, Netherland, Belgium and Northern Germany. The 10m wind speed exceeds 20m/s in several regions during the passage of the cyclone.

Fig. 7a shows the time-averaged power dissipation index in the various runs and the change pattern. The highest impact of winter storms is as expected at the coasts. There is an increase in northern Europe for both the near future and end of century scenarios. In the frequency distribution of this index displayed in Fig. 7b we can verify this outcome but there is an increase of extreme cases only in the near future run. This result could possibly be linked to inter-decadal variability for wind speed.

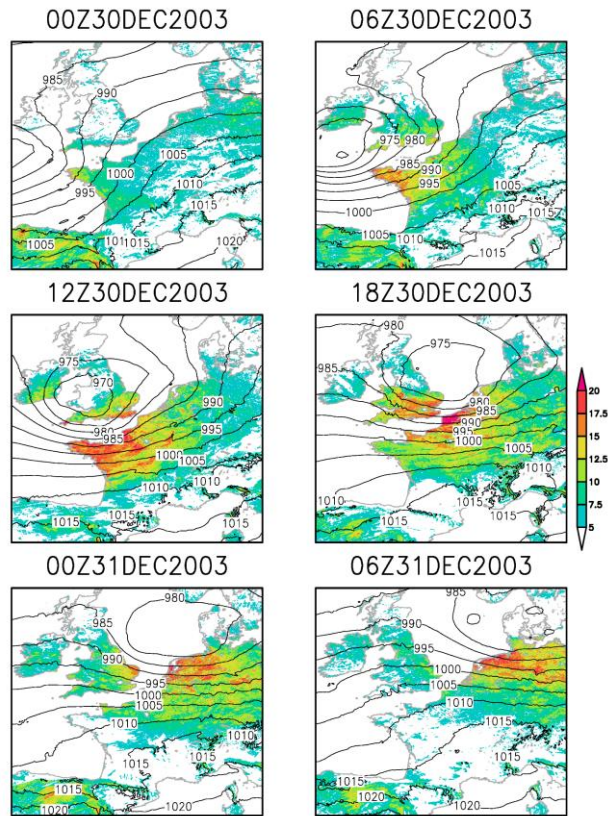


Figure 6: Selected snap-shots of the NWE-3 simulation displaying 10m wind speed (coloured shadings, m/s) and sea level pressure (hPa). These figures show the passage of a very intense winter storm.

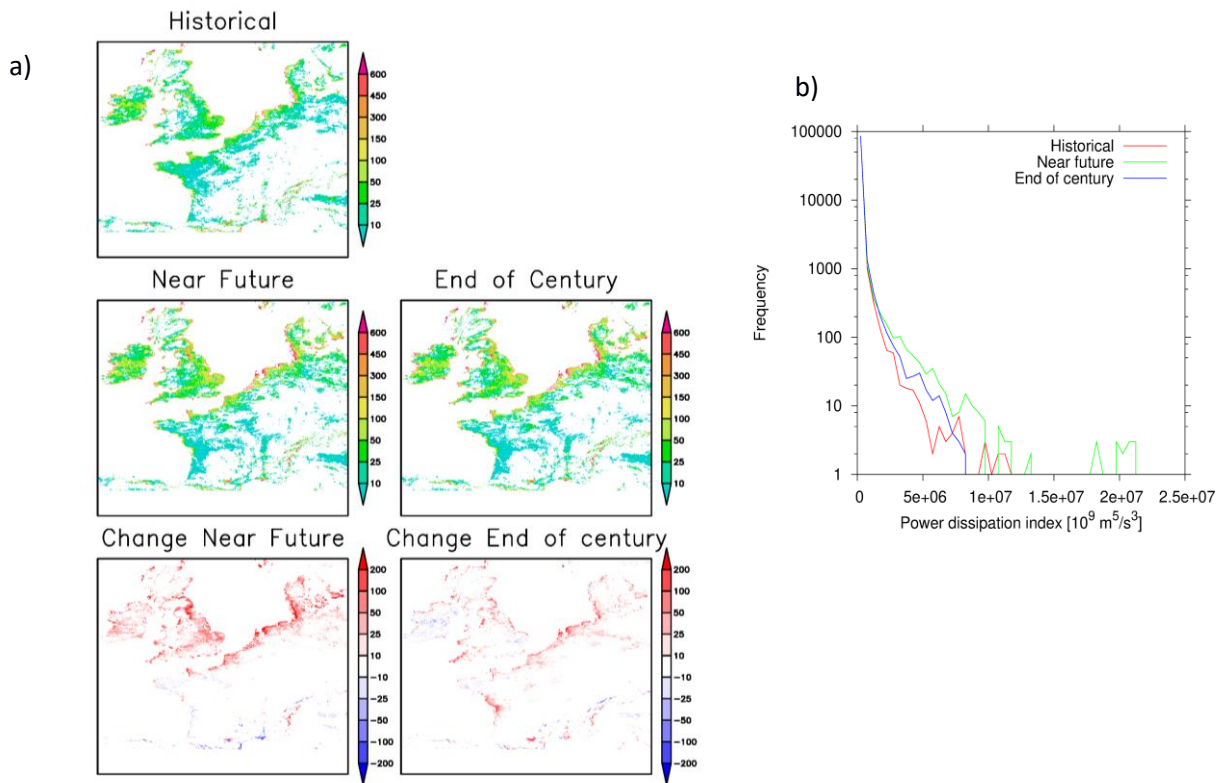


Figure 7a) Time-averaged power dissipation index for the various simulations and its climate change, b) frequency distribution of the power dissipation index for the various simulations.

### 3.3.1.2 Precipitation changes in NWE-3 domain (multi-model analysis)

We summarize the results of Berthou et al. (in prep.) in this section. We used the NWE-3 domain (KNMI, CNRM), NEUR-3 domain (SMHI/DMI/FMI), and REU-2 domain (ETHZ, MOHC) simulations to look at precipitation changes within winter storms. Although these domains are different, they all cover a sub-region of northern Europe where winter mean precipitation is expected to increase. This increase is linked with both a projected extension of the storm track over this region and an increase in precipitation per storm (Catto et al. 2019).

Kendon et al. (2020) showed larger increases of mean winter precipitation with a single CPM driven by a perturbed parameter global and regional ensemble (using a single MOHC model), and explained 60% of this signal by the fact that shallow convection (showers) were advected over land in the CPM, and not in the RCM, showing larger increases over land. We now employ this 5-member EUCP ensemble of RCM/CPM pairs to investigate whether this result is also found with other models. Fig. 8 shows that the other CPMs agree with the mean change of their parent RCM, unlike the MOHC model. Nevertheless, weather case studies showed that CPMs represent many winter storm precipitation processes better: shallow convection in the cold sector/dry intrusion overlaying a warmer surface, slantwise convection releasing conditional symmetric instability associated within fronts (CSI), better representation of frontal structures, dry intrusion overrunning the warm sector, embedded convection in warm conveyor belt and cold fronts. We therefore used our ensemble to better understand in-storm hourly precipitation changes. We focused on in-storm precipitation changes to avoid natural variability in the number of storms. We still have the effect of natural variability in the dynamical strength and nature of storms, so we selected the end-of-century time-slice to maximize the climate change signal.

We tracked all the extratropical cyclones entering the driving RCM domain with the widely used feature tracking package called TempestExtremes (Ullrich et al. 2021; Zarzycki et al. 2017). We selected all the tracks within 2 degrees inside the CPM domain (boxes in Fig. 8).

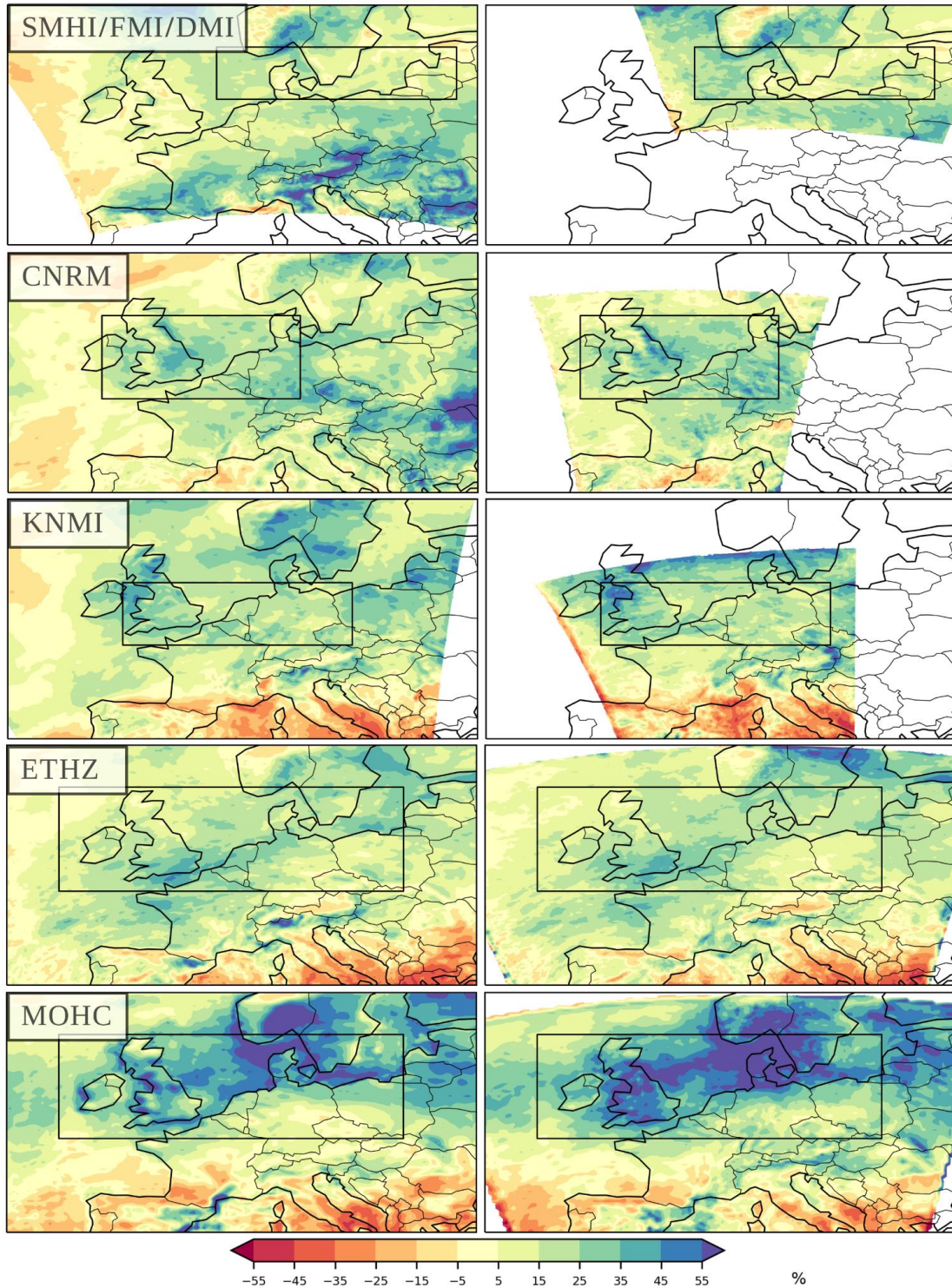


Figure 8: Percentage change in mean winter precipitation at the end of the century compared to the reference period. Left: convection-parameterised RCM, Right: convection-permitting models. The box shows where extratropical cyclone tracks are selected.

Figure 9 shows a random sample of storms in the present-day simulations. We used mean sea level pressure (MSLP), precipitation and wet bulb potential temperature within a 10 degree radius of the MSLP minima to define different storm sectors, as explained in this figure.

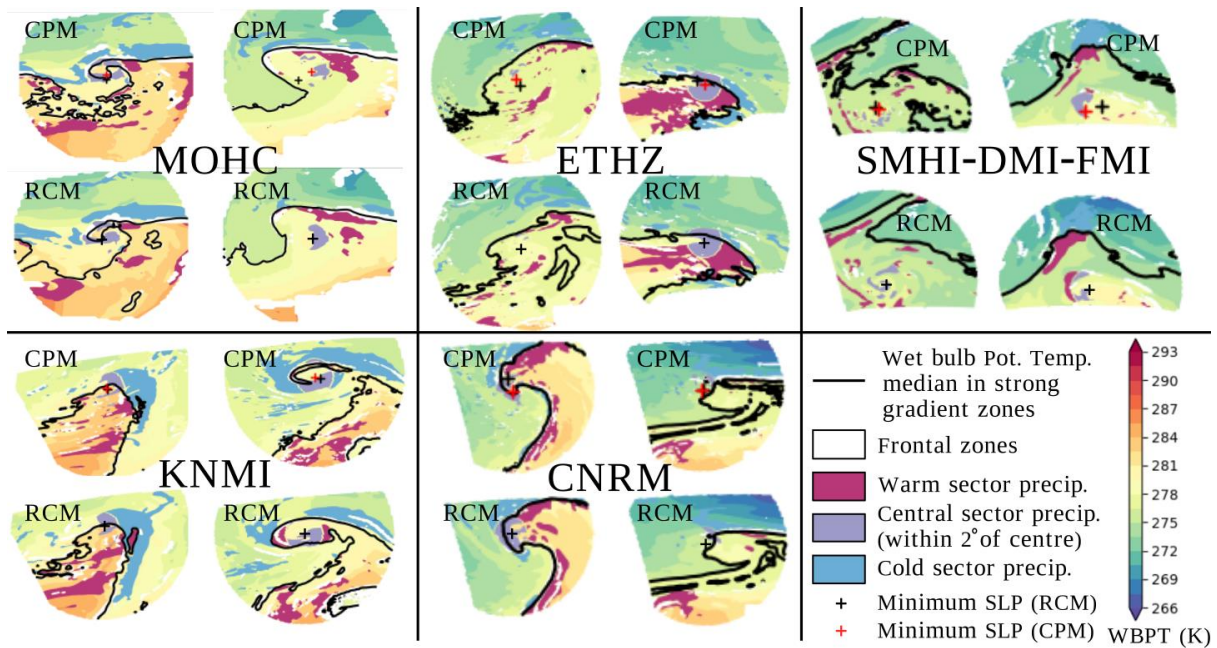


Figure 9: Examples of storms selected for each model: two different storms (left/right) in the CPM (top) or RCM (bottom). Storm sector definitions are explained in the legend, frontal zones are defined as areas with the norm of Wet Bulb Potential Temperature gradients stronger than 4K/110km (or 5km/110km for MOHC model on a 25km grid)

Figure 10 shows that mean precipitation increases in future winter storms, due to similar occurrences of weak precipitation but increased moderate and intense precipitation. This increase mostly comes from the warm sector of storms, and that CPMs agree on this fact, unlike RCMs. Nevertheless, differences between CPM and RCM are smaller than inter-model differences, because their warming levels in the warm sector of storms and the changes in dynamical strength of storms are different (not shown here). In the MOHC model, the CPM increases precipitation more than the RCM in both the warm and cold sector. The warm sector increase is linked with more convection there (shown below) and is coherent with other CPMs showing the largest differences with the RCM in this sector. The larger increase in the cold sector is likely linked with a deficiency in the RCM to advect showers over land (Kendon et al. 2020), but this larger increase is particular to this model and cannot be generalised. This may be because it is the only model to show larger cold sectors in future storms (not shown here), possibly linked with an increase in Shapiro-Keyser storms in this model, with a larger cold sector (Manning et al. 2021). It may also be particular to the convection scheme used in the MOHC RCM. Because the temperature ranges in future winter storms reach similar values to autumn ones in the most pessimistic model (MOHC), we compared future winter storms with present-day autumn storms in Figure 11 for this model. Intense (>5mm/h) and heavy (>10mm/h) precipitation have similar frequencies in the warm sector of future winter storms as in present-day autumn storms. Both convective available potential energy and convective inhibition increase in the same WBPT bins (Fig. 10), indicating that some of this increase in precipitation rates is due to convection. Nevertheless, the CAPE and CIN levels remain lower than in present-day autumn storms, possibly due to higher relative humidity in winter storms which maintains lower CIN values (Chen et al. 2020), or possibly slantwise convection having a larger share compared to vertical convection, but we did not have enough model output to verify this.

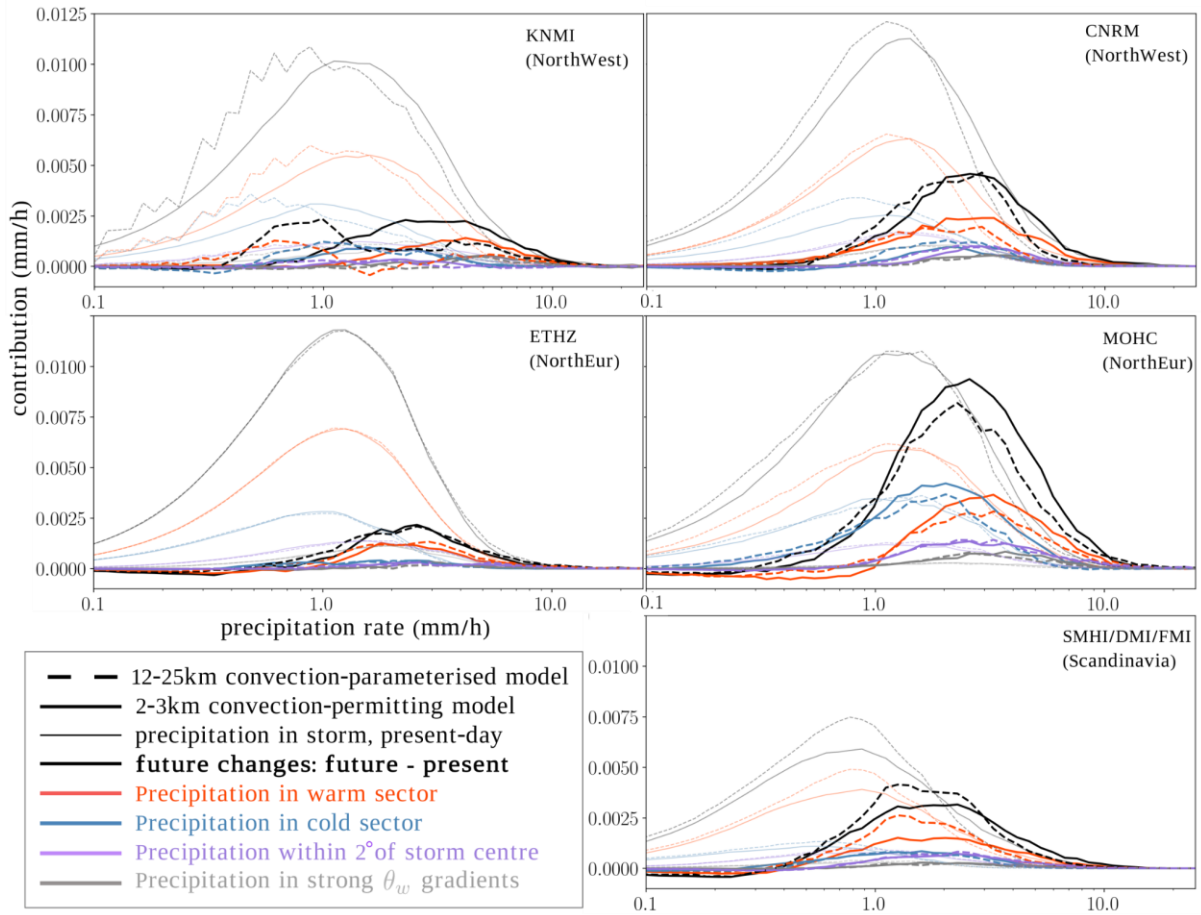


Figure 10: Precipitation contribution to the mean within storms (frequency  $\times$  value of bin, using exponential bins defined in Berthou et al. (2019)). This way, the area under the curve is mean precipitation for the present-day (thin lines) and end-of-century mean precipitation increase (future-present, thick lines). Contribution from all points in storms (black), points in warm sector (red), cold sector (blue), central sector (purple) and strong WPBT gradients (grey), as defined in Fig.9. Plain line is for CPM, dashed line for RCM.

We further showed that mean hourly precipitation in future winter storms reaches larger values than autumn storms, and explained this by the fact that present-day autumn storms have lower relative humidity in their warm sector (not shown), and less weak precipitation (blue curve in Fig. 10). However, moderate to intense precipitation increases with temperature at the same rate between autumn and future winter storms (not shown).

To conclude, the larger increase in mean precipitation in winter storms in the MOHC CPM is not found in other RCM/CPM pairs. We therefore recommend to look at multi-model ensembles when possible. We showed that CPMs are useful tools to better understand changes in intense rain rates and fine-scale processes in winter storms, and that they agree better on changes in precipitation in the warm sector of winter storms. Nevertheless, levels of warming within the warm sector of storms and dynamical strength of storms are the largest factor to explain mean and intense precipitation changes in storms, for winter storms where relative humidity remains high. Therefore, the differences between RCMs are larger than the RCM/CPM differences for this type of events.

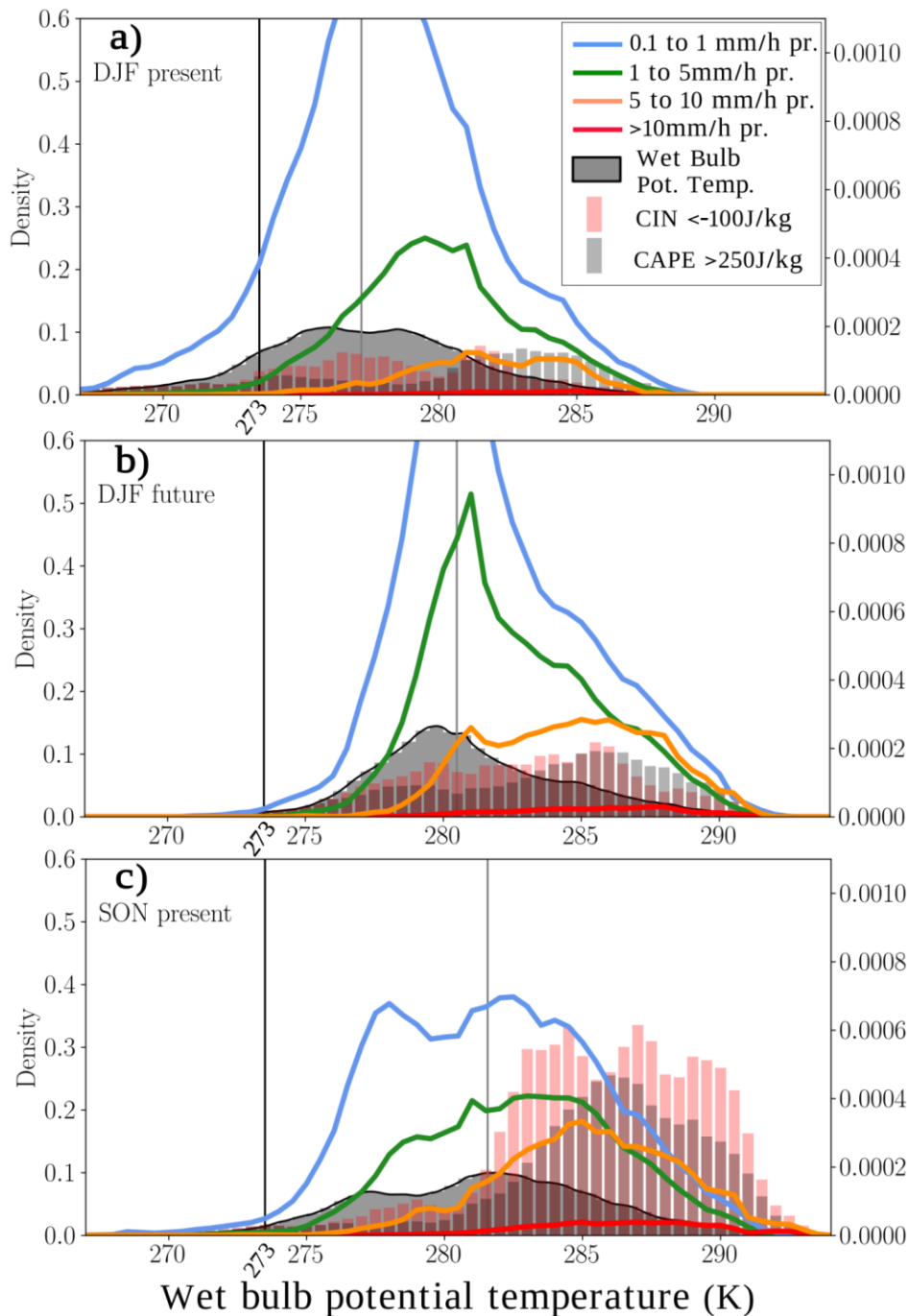


Figure 11: Density of 850hPa Wet bulb temperature (black line with grey shading, left axis). Occurrence of low (0.1 to 1mm/h) and moderate (1 to 5mm/h) precipitation scaled by 1/10; intense (5-10mm/h) and heavy (>10mm/h) precipitation; CAPE (>250J/kg) and CIN (<-100J/kg), both scaled by 1/10, all binned by WPBT values and normalised by the number of points in all storms, on the native grid in the MOHC CPM. a) present-day winter storms, b) future end-of-century winter storms and c) present-day autumn storms.

### 3.3.2 CEU-3: Continuous heavy rain

Continuous heavy rain cases are analysed in the REMO-NH (GERICS) simulation of the CEU-3 domain.

To identify continuous heavy rain, we used the following method

- The number of consecutive days with more than 1mm precipitation is calculated.
- The accumulated precipitation of the period with consecutive precipitation days is determined

- The precipitation mass of those grid points which have at least 2 consecutive days of precipitation and an accumulated precipitation of more than 20mm is computed.

Fig. 12 shows time series of the precipitated water mass determined with the aforementioned method for the historical and near future periods. There is no accentuated annual cycle as it is seen for the power dissipation index (cf. Fig. 5). Therefore, heavy rain can appear in all seasons. Comparing near future with historical suggests a slight decrease of extreme cases.

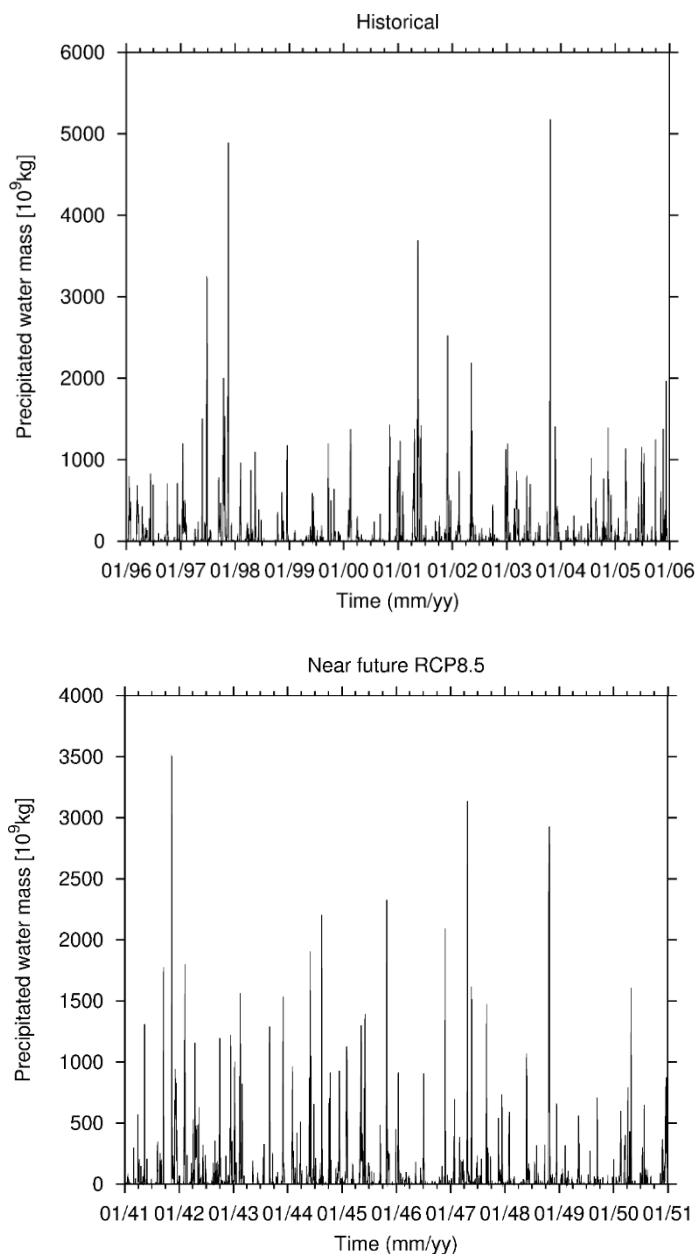


Figure 12: Time series of precipitated water mass deduced from a) the historical run (1996-2005) and b) the near future run (2041-2050) for the CEU-3 domain.

Fig. 13 shows a case with high continuous heavy rain. It is associated with a Mediterranean low that moves northward. This is the Vb weather pattern (van Bebber 1891) that is often responsible for severe floods in central Europe (e.g., Grams et al. 2014).

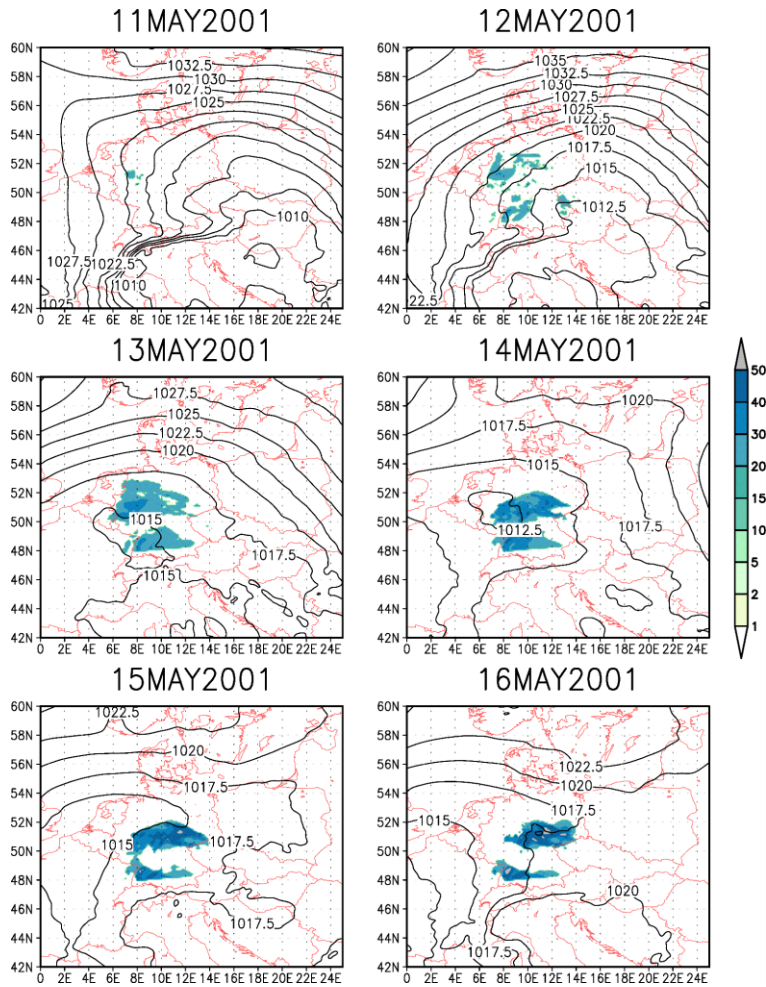


Figure 13: Selected snap-shots of the CEU-3 simulation displaying accumulated precipitation (mm) of consecutive days and sea level pressure (hPa). These figures show a continuous heavy rain case with high precipitated water mass.

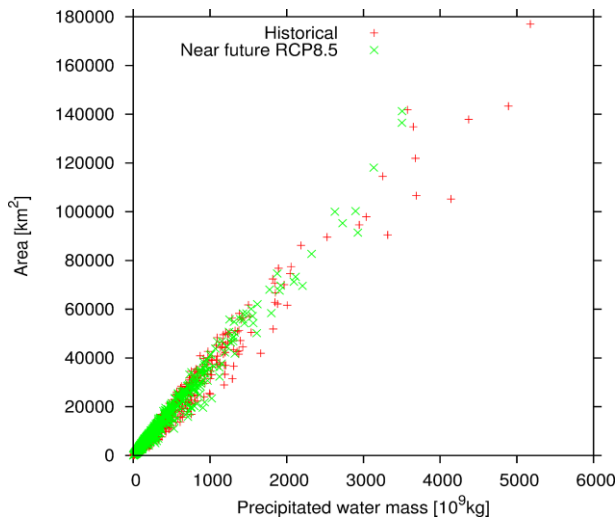


Figure 14: Scatter diagram: precipitated water mass versus area for the historical (1996-2005) and near future run (2041-2050).

Fig. 14 shows a scatter diagram for the historical and near future runs. We can detect a decrease of maximum precipitation mass in the extreme cases in the near future run. However, this is not

statistically robust given the short time integration period. Furthermore, we only evaluated one model and other models may give different answers.

### **3.3.3 SWE-3: Droughts**

Frequency index representing droughts (Mishra et al. 2010) as consecutive dry days (CDD) is assessed over the Iberian peninsula (included in the South-West domain – SWE-3), as defined within the H2020 EUCP project. The CDD index is calculated from the results of climate simulations run with the regional climate model COSMO-CLM at different spatial scales (~12 km and ~3 km) over 10 year-long periods in the evaluation experiment and then historical, and near future experiments under RCP8.5 scenario. The simulation at 3 km of resolution was run in convection permitting mode and nested into the one at 12 km of resolution over the Euro-Cordex domain. CDD is the maximum number of consecutive days with precipitation <1mm. The available observation datasets, used as reference in this study, are SPREAD at 5 km of resolution (SPREAD, 2017) and SPAIN02 at 12 km of resolution (Herrera et al., 2012). A comparison among observations, results from regional climate model (RCM) and convection permitting model (CPM) for evaluation runs is presented in Figure 15. The CDD index has a spatial distribution with a strong north-south gradient, revealed by observations and both climate simulations, also in agreement with previous studies (Domínguez et al. 2013). The South part of the peninsula has the highest observed values, with maximum values >100 d/year, reflecting the summer dry period. Metrics as mean value, minimum value, maximum value and standard deviation have been assessed in the following tables. Table 3 shows the metrics for CDD over Spain (common domain) for the evaluation experiment (2000-2009) highlighting that the metrics of CPM are much closer to the observations (especially with Spread5 dataset). The CPM results highlight that the maximum number of consecutive dry days for the period 2000-2009 is in the mean of around 62 days with standard deviation of around 25 days. The latter values overestimate the CDD metrics if compared with observations. SPREAD-5 dataset has a mean of around 54 days with standard deviation of around 24 days and SPAIN02 has a mean of around 43 days with standard deviation of around 17 days. A comparison between RCM and CPM for past and near future spans is presented in Figure 16. Table 4 shows the metrics for CDD for the historical experiment (1996-2005) while Table 5 shows the metrics for the near future experiment (2041-2050). The CPM results highlight that the maximum number of consecutive dry days for the period 1996-2005 is in mean of around 49 days with standard deviation of around 25 days; for the near future (2041-2050) it is projected to be of around 57 days with standard deviation of around 29 days. The RCM results highlight that the maximum number of consecutive dry days for the period 1996-2005 is in mean of around 70 days with standard deviation of around 39 days; for the near future (2041-2050) it is projected to be of around 77 days with standard deviation of around 38 days.

Figure 17 shows the box plots for consecutive dry days in historical experiment and near future from CPM results. It is projected that consecutive dry days will increase in near future both in mean values and extremes associated with a change in distribution. In other words, although the mean value of CDD number would not increase significantly from historical period to the near future one, an extended area of the peninsula would be affected by higher values of CDD in the future compared with the historical asset, reaching values higher than 130 CDD day/year.

Table 3: Metrics on CDD index over Spain (common domain) for the evaluation experiment (2000-2009).

EVALUATION 2000-2009	CDD (d/year)			
	MEAN	MIN	MAX	STD
OBS – SPAIN02-12	43.43	17.20	98.90	16.81
OBS – SPREAD-5	54.06	13.10	136.20	24.44
CPRCM-3	61.68	19	147.10	25
RCM-12	80.53	22.7	142.90	27.09

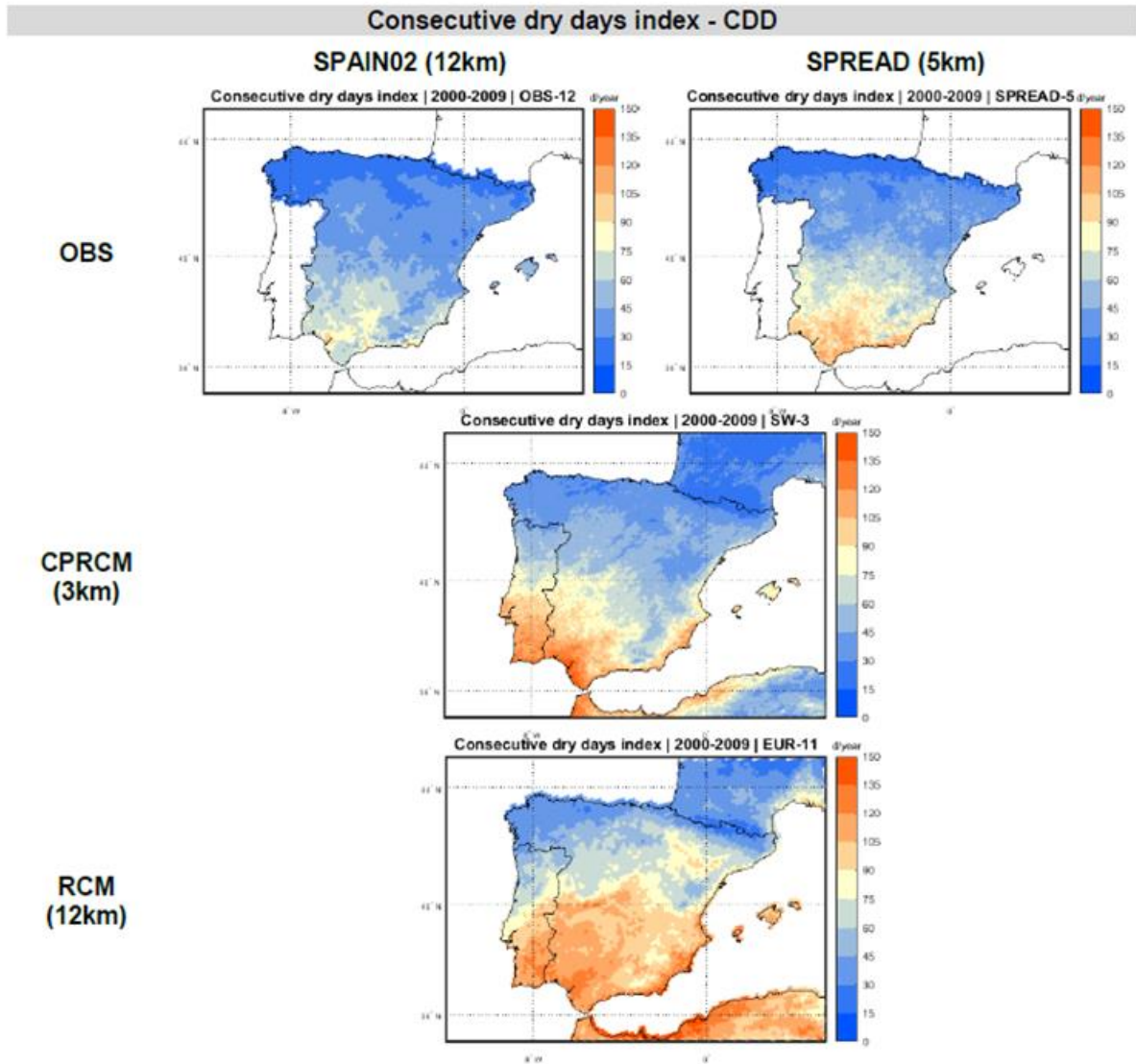


Figure 15: Consecutive dry days index for the period 2000-2009 over SWE-3 domain.

Table 4: Metrics on CDD index over SWE-3 domain for the historical experiment (1996-2005).

HISTORICAL 1996-2005	CDD (d/year)			
	MEAN	MIN	MAX	STD
CPRCM	49.18	14.40	155.70	25.17
RCM	69.68	16.90	194.60	38.57

Table 5: Metrics on CDD index over SWE-3 domain for the near future experiment (2041-2050).

NEAR FUTURE 1996-2005	CDD (d/year)			
	MEAN	MIN	MAX	STD
<b>CPRCM</b>	57.13	13.80	180.10	28.94
<b>RCM</b>	77.17	15.30	203.50	38.47

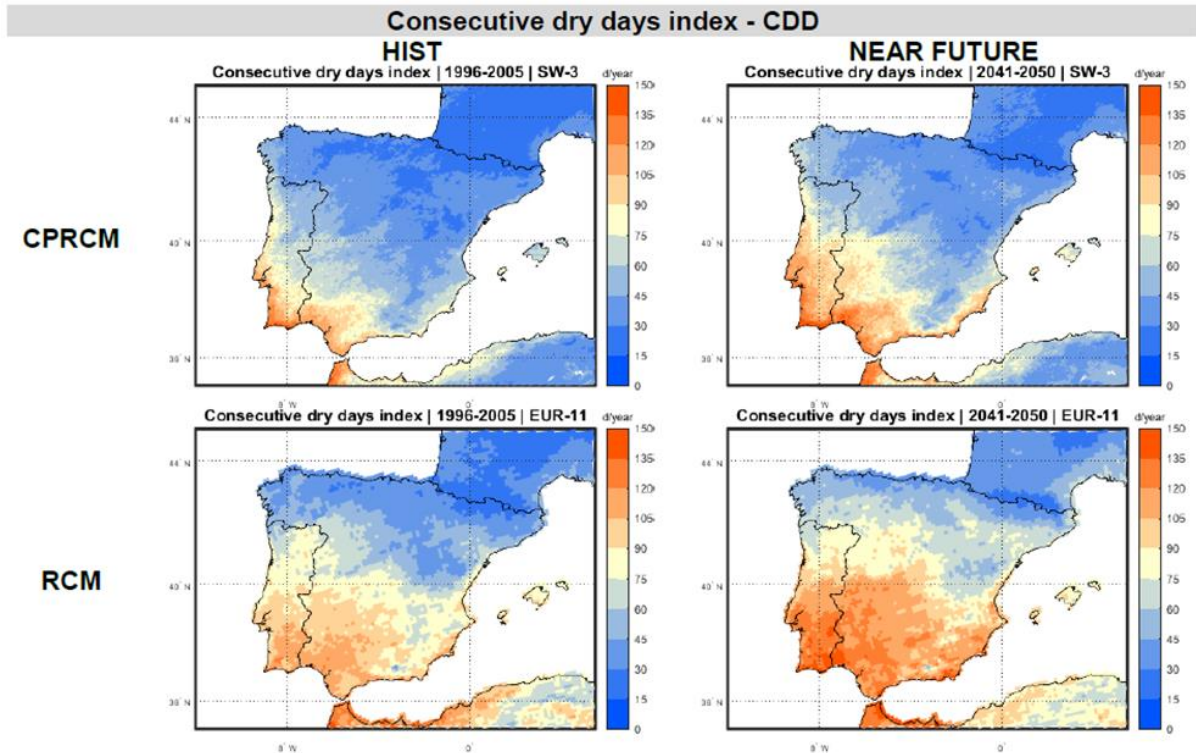


Figure 16: Comparison between historical period and near future for consecutive dry days index over SWE-3 domain.

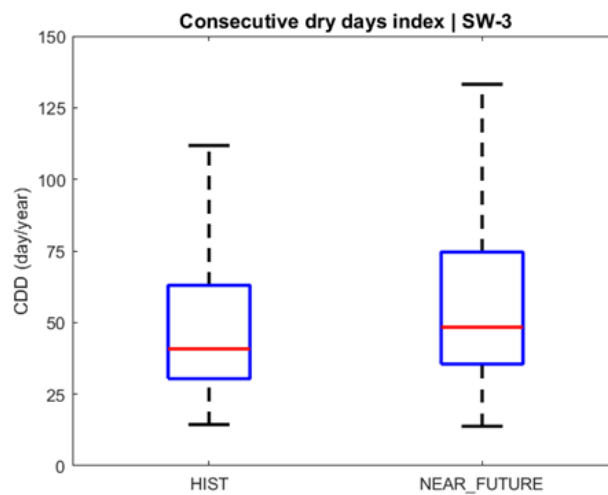


Figure 17: Box plots for consecutive dry days in historical experiment and near future from CPM results.

### **3.3.4 ALP-3: Fall Mediterranean Heavy Precipitation Events (CNRS-CNRM)**

#### **3.3.4.1 Aim of the study**

The northwestern Mediterranean is affected by High Impact Weather Events (HIWE) called Heavy Precipitation Events (HPEs), occurring mainly during the fall season (Ducrocq et al. 2008; Nuisser et al. 2008, 2011). With rainfall accumulations greater than 100 mm recorded in less than a day and often within just a few hours, these extreme events lead to devastating flash flooding and landslides that may cause widespread destruction and even fatalities. Therefore, societal needs for information about the future evolution of these high impact weather events are high.

The climate rainfall extremes involved in Mediterranean HPEs are essentially produced through small-scale to meso-scale convective motions in the atmosphere, leading to short duration precipitation extremes. Convection Permitting Regional Climate Models (CPMs) have shown a step-change in the quality of reproducing these short duration precipitation extremes (Ban et al. 2021) and especially fall Mediterranean HPEs (Fumière et al. 2020, Berthou et al. 2020, Caillaud et al. 2021, Pichelli et al. 2021) with respect to lower-resolution climate models such as GCMs or RCMs.

Moreover, this good behaviour of CPMs allows it to go beyond the basic Eulerian statistical approach and to set up an object-oriented Lagrangian approach in order to take into account the spatial and temporal connections that may exist within a given event. The object-oriented approach has already been used at CNRS-CNRM to demonstrate the ability of the CNRM-AROME CPM to represent French Mediterranean HPEs in terms of location, frequency, intensity, frequency, duration, area and severity by comparison with high resolution observation (Caillaud et al. 2021). The same approach will be applied in this study to investigate the near future changes in Mediterranean HPE characteristics within the EUCP CPM ensemble.

#### **3.3.4.2 Methodology**

The object-oriented approach used here to study HPEs is based on the precipitating system detection and tracking algorithm developed at CNRM (Morel and Senesi 2002a). More information about the tracking algorithm can be found in Caillaud et al (2021).

The tool is applied to the 1-h accumulated precipitation fields of the nine CPMs of the EUCP ensemble (cf. Tab. 6) interpolated on the regular 3-km resolution ALP-3 domain (cf. Fig. 18). The tracking is done both for the 10-year historical period (1996-2005 except for UKMO-UM: 1998-2007) and for the 10-year near future period (2041-2050 except for UKMO-UM and RegCM4: 2040-2049) simulations driven by different GCMs under the RCP8.5 scenario.

The studied period is an extended fall season (from September to December), the period in which most of the HPEs occur in the Mediterranean region (Ricard et al. 2012).

Firstly, the changes in spatial density of the Mediterranean HPEs are explored, selecting convective precipitation by only accounting for systems trajectories with mean intensities above 10 mm/h. Then, the focus is on the French Med area (cf. Fig. 18). Following Caillaud et al (2021), the tracks are selected crossing the French Med area, with mean intensities above 10 mm/h and occurring during days with 24-h accumulated precipitation exceeding the 100 mm threshold at least once over the French Med area.

Table 6: Modelling systems used by the participating groups.

NAME	GROUP	CPM	dx (km)	RCM	RCM domain / dx (km)	GCM	CMIPx
CMCC-COSMO	CMCC	CCLM	3	CCLM	EUR-11/12	EC-Earth r12	CMIP5
CNRM-AROME	CNRM	AROME41t1	2.5	ALADIN63	EUR-11/12	CNRM-CM5 r1	CMIP5
HClim-AROME	DMI/SMHI	HCLIM38-AROME	3	HCLIM38-ALADIN	Europe/12	EC-Earth r12	CMIP5
KNMI-AROME	KNMI	HCLIM38-AROME	2.5	RACMO	Europe/12	EC-Earth r14	No
ETHZ-COSMO	ETHZ	CCLM-GPU	2.2	CCLM	Europe/12	MPI-ESM-LR r1	CMIP5
GERICS-REMO	GERICS	REMO	3	REMO	Europe/12	MPI-ESM-LR r3	CMIP5
ICTP-RegCM	ICTP	RegCM4	3	RegCM4	Europe/12	HadGEM2-ES r1	CMIP5
IPSL	IPSL	WRF <sup>a</sup> RegIPSL <sup>b</sup>	3 <sup>a</sup> 3 <sup>b</sup>	WRF <sup>a</sup> RegIPSL <sup>b</sup>	Europe/15 <sup>a</sup> MEDCORDEX/18 <sup>b</sup>	IPSL-CM5-MR r1 <sup>a</sup> IPSL-CM6 r1 <sup>b</sup>	CMIP5 <sup>a</sup> CMIP6 <sup>b</sup>
UKMO-UM	UKMO	UM	2.2	HadGEM3-GC3.1-N512 (HiresMIP)	Global/25	HadGEM2-ES r1	AMIP-CMIP5 SST

<sup>a</sup>For ALP region run

<sup>b</sup>For SWE region run

### 3.3.4.3 HPEs spatial density

**Preliminary evaluation:** The objective of this study is not to assess in depth the model or simulation behaviour. This has been done in previous deliverables (D3.2 and D3.3). However, we perform here a preliminary evaluation in studying some characteristics of precipitating systems. Figure 19 presents the spatial distribution of the mean numbers of cells per year above 10 mm/h for the ten fall seasons for the historical period. The CPMs generally behave well in terms of the number and geographical positioning of the main centers. Indeed, the regions known to be the most affected by fall Mediterranean HPEs (that means the southeast of France with in particular the Cevennes region and Corsica, the Italian western coast with the Ligurian region, the region from the Carnic Alps to Croatia) are well represented by all the models. Biases in the number of cells (overestimation or underestimation or both depending on the models) are observed, although it is difficult to attribute the origin of these biases solely to the CPM or to the driving conditions given by the GCM. Moreover, the ten years of historical simulations are not directly comparable to the ten years of observations. This first evaluation allows to conclude that all the CPMs are suitable for the study of Mediterranean HPEs.

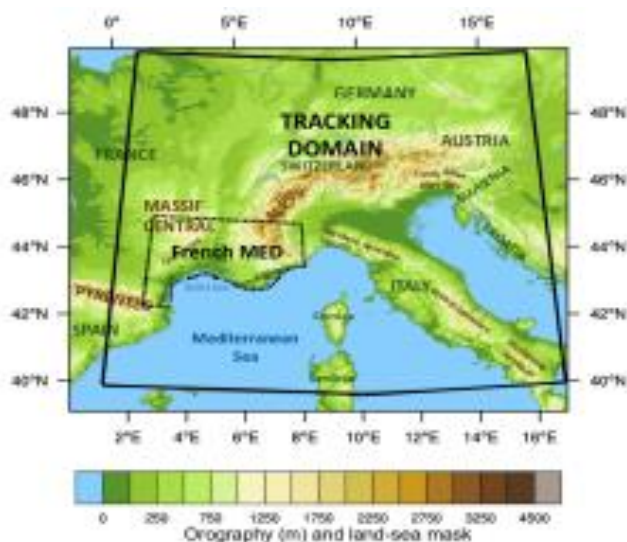


Figure 18: CNRM-AROME topography for the pan-Alpine domain. Delimited by black lines, the regular ALP3 domain is used as the tracking domain and the French Med area is delimited by black dotted lines.

**Near future evolution (2041-2050):** Focusing on the near future changes in spatial density (cf. Fig. 20), the dispersion in possible futures is rather large when looking at the nine vignettes of the different models. Even two models driven by the same GCM (such as ICTP-RegCM and UKMO-UM) show different expected changes and ranges of values. However, the multi-model ensemble mean and especially the model agreement index show a rather good agreement for an increase of the number of events and their extension over the eastern part of the southeast of France, over the western Italian coast and over the region from the Carnic Alps to Croatia. A decrease over the Gulf of Lions sea area is projected by the ensemble, but with a weaker agreement level.

#### 3.3.4.4 HPEs characteristics over French Mediterranean Area

**Quick evaluation:** The maximum Intensity Duration Frequency (IDF) plot (cf. Fig. 21) considers the fall HPEs concerning the French MED area (cf. Fig. 18) for the historical period. The nine CPMs represent quite well the observed pattern of the IDF. Some differences between models can be seen with higher simulated intensities for some of them (such as ICTP-RegCM or UKMO-UM) or longer duration (for KNMI-AROME or Hclim-AROME), but it is not really possible to gather the IDF plots by model family or by common driving GCM. The number of tracks can also differ between models (less than 1000 for GERICS-REMO and more than 3000 for CNRM-AROME or ETHZ-COSMO with an ensemble mean of 2106 to be compared with an observed value of 2527 for a ten year period).

**Near future evolution (2041-2050):** The changes in IDF distributions between historical and near future periods (cf. Fig. 22) are rather patchy and not really informative when considering each model alone. UKMO-UM is nearly the only one to show a clear signal with shorter and more intense events. However, the multi-model ensemble shows quite a good agreement for an increase in maximum intensity for all duration for events stronger than 25mm/h. Below this intensity threshold, event lifetime is shortened despite a lower degree of agreement.

The evolution in the number of tracks between historical and near future periods (given at the bottom right of the model's vignette) shows a large dispersion between models, ranging from -19 to +37%, but a large majority of models (7/9) agrees that the number of trajectories will increase in the near

future period.

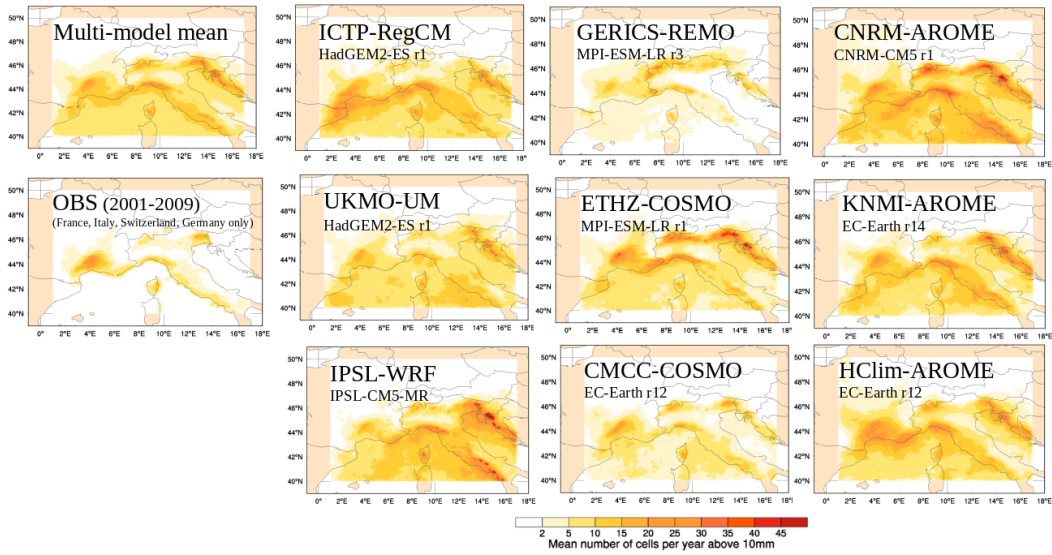


Figure 19: Spatial density of cells above 10mm/h (number per year) during extended fall (SOND) for the historical period (1996-2005) for the 9 CPMs (driving GCMs are given under the model name), the multi-model ensemble and the observations (2000-2009, available only over lands of France, Italy, Switzerland and Germany).

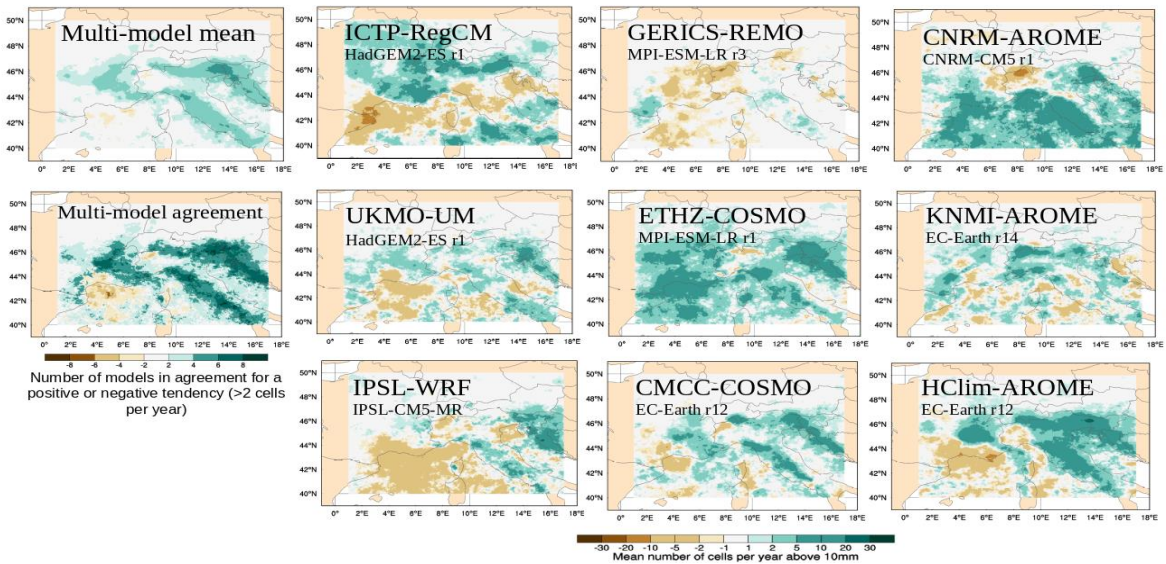


Figure 20: Raw differences of spatial density of cells (number per year) above 10mm/h during extended fall (SOND) between the mid century period (2041-2050) and the historical period (1996-2005) for the 9 CPMs and the multi-model ensemble. The number of models in tendency agreement is also given, considering only changes in number of cells above two.

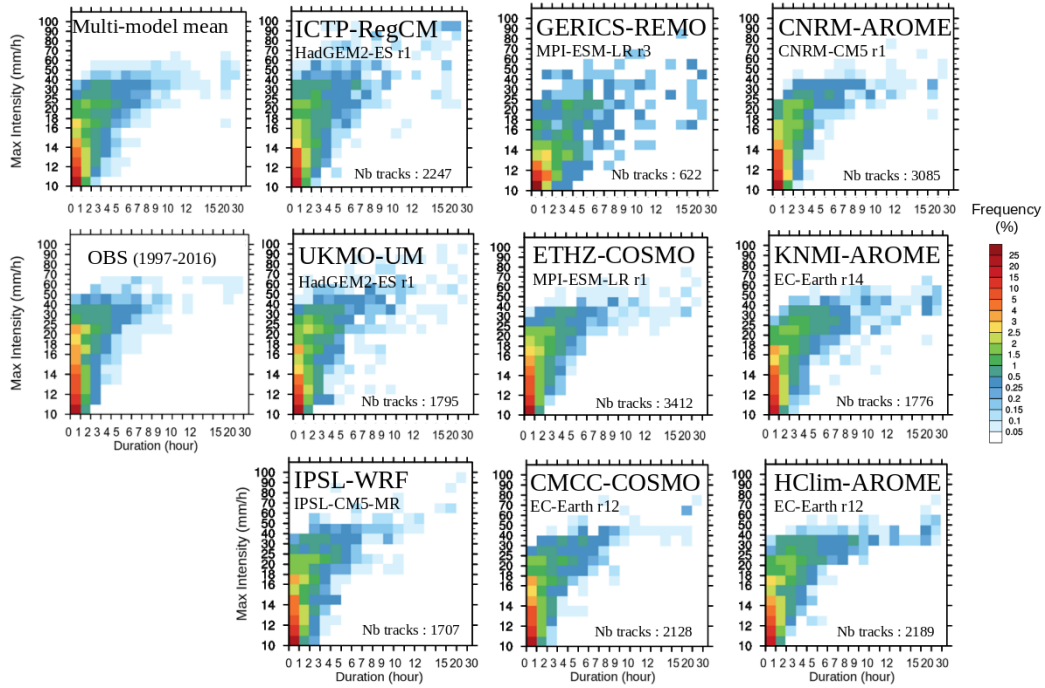


Figure 21: Intensity duration frequency (IDF) plot considering all tracks of cells above 10 mm/h occurring during days exceeding 100 mm/day in the French MED area during the extended fall (SOND) for the historical period (1996-2005) for the 9 CPMs (the number of tracks is given for each model), the multi-model ensemble and observations (1997-2016).

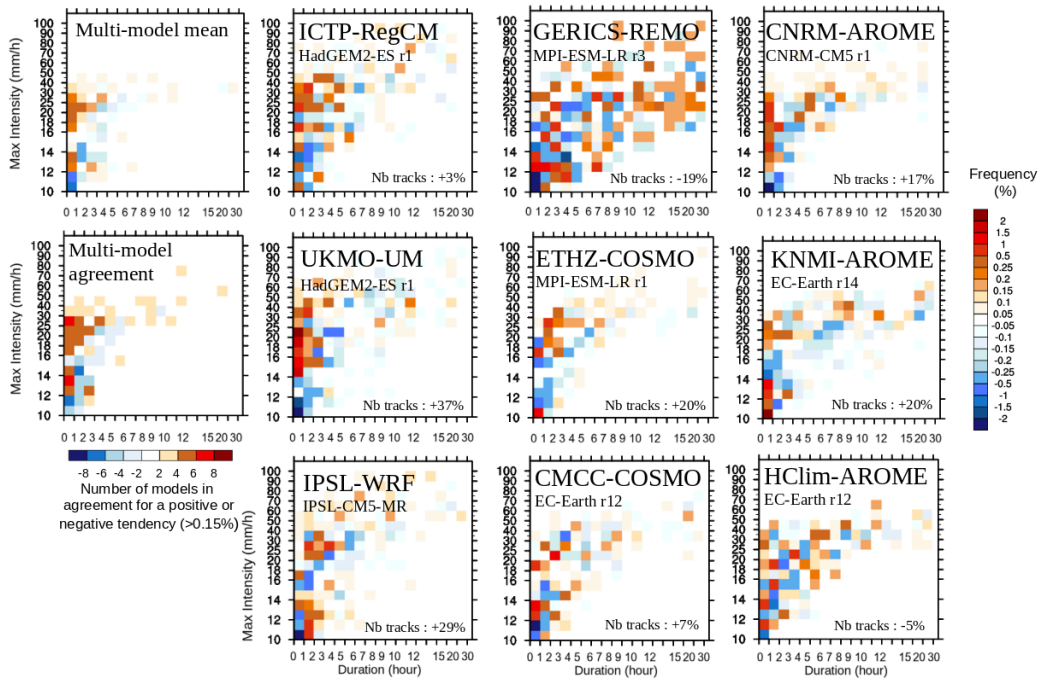


Figure 22: Differences of intensity duration frequency (IDF) plot considering all tracks of cells above 10 mm/h occurring during days exceeding 100 mm/day in the French MED area during the extended fall (SOND) between the mid century period (RCP85 2041-2050) and the historical period (1996-2005) for the 9 CPMs (the evolution of the number of tracks is given for each model) and the multi-model ensemble. The number of models in tendency agreement is also given, considering only changes in frequency above 0.15%.

### **3.3.4.5 Conclusion**

To our knowledge, this is the first time that a CPM ensemble (9 members) is analyzed using a Lagrangian approach that allows to better characterize the spatio-temporal variability of the Mediterranean Heavy Precipitation Events (HPEs) than more classical Eulerian statistics as applied in previous EUCP deliverables and in the literature (Ban et al. 2021, Pichelli et al. 2021).

For the historical period and despite some differences between the various model chains, the EUCP CPMs ensemble confirms the general ability of CPMs to represent well the location, intensity and duration of fall Mediterranean HPEs whatever the CPM used and whatever the driving GCM. This confirms in multi-model and in the historical running mode, the results obtained with CNRM-AROME and in the evaluation mode in Caillaud et al. (2021).

Giving a conclusion on the evolution of these extreme events for the near future period is made difficult by the large dispersion among model simulations. However, consensus is reached on an increase in the number of events and on their extension over the eastern part of the southeast of France, over the western Italian coast and over the region from the Carnic Alps to Croatia. The multi-model ensemble also shows quite a good agreement for an increase in maximum intensity for all duration for the highest intensity events in the French Med area.

We are however fully aware that the ensemble used here (9 future runs, 6 independent CPMs, 5 independent GCMs, 10-year long runs) is relatively small with respect to the study of the evolution of extreme precipitation events for the near future period. Indeed, we are facing a large diversity of uncertainty sources (GCM choice, member choice, internal variability, CPM choice, intermediate nesting strategy) and a very small number of years to assess them. At the first order, the differences in dynamical changes proposed by the driving GCMs giving the propitious large-scale conditions leading to HPEs seem to play an important role in the CPMs' spread. Differences in behaviour between the high resolution models is also detectable for some variables. Finally, the large internal variability given the rather short 10-yr simulation periods when focusing on rare extreme events and the relatively small forced change to the near future period lead to a small signal over noise ratio, which has been already underlined in the deliverable D3.3. In the coming years, as the CPMs and the computer power develop, larger ensembles of longer simulations will likely be available which will contribute to obtaining more robust results when assessing the future evolution of rare events.

This study could be extended by focusing on other HPEs characteristics such as the size or the speed of the cells and also on other geographical areas with a wider consensus between models on the sign of the expected change (such as Italian coast or Croatia).

### **3.3.5 NEU-3: Polar Lows**

Polar lows are intense mesoscale cyclones which develop when cold polar air flows above a relatively warmer sea surface. Polar lows are studied in the NEU-3 REMO-NH simulations by GERICS. These are identified with the method by Zahn and von Storch (2008). However, as a difference we do not apply spatial filtering of the sea level pressure field before identification. It seems that unfiltered pressure fields at convection permitting scale already show well defined minima in the center of the polar lows. Furthermore, cyclones originating south of 60°N are not identified as polar lows.

Fig. 23 shows the identified polar low tracks for both REMO-NH simulations. In the historical and near future runs 101 and 97 polar low tracks are found, respectively. Most of the polar low tracks appear in the Norwegian Sea. Only a few cases show up in the Barent Sea. This happens likely due to the close proximity of the model boundary. No polar lows originate in the Baltic Sea.

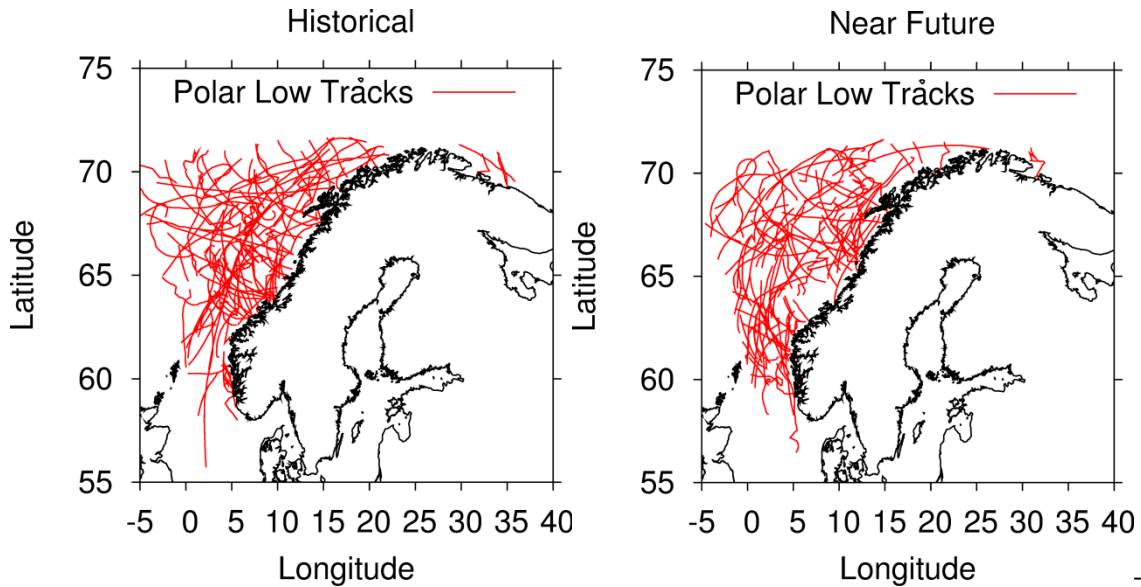


Figure 23: Identified polar low tracks in the historical (left panel) and near future (right panel) simulations.

Fig. 24 shows the number of identified polar low tracks as a function of time. Obviously, polar lows arise in the winter and early spring seasons. There is also considerable interannual variability.

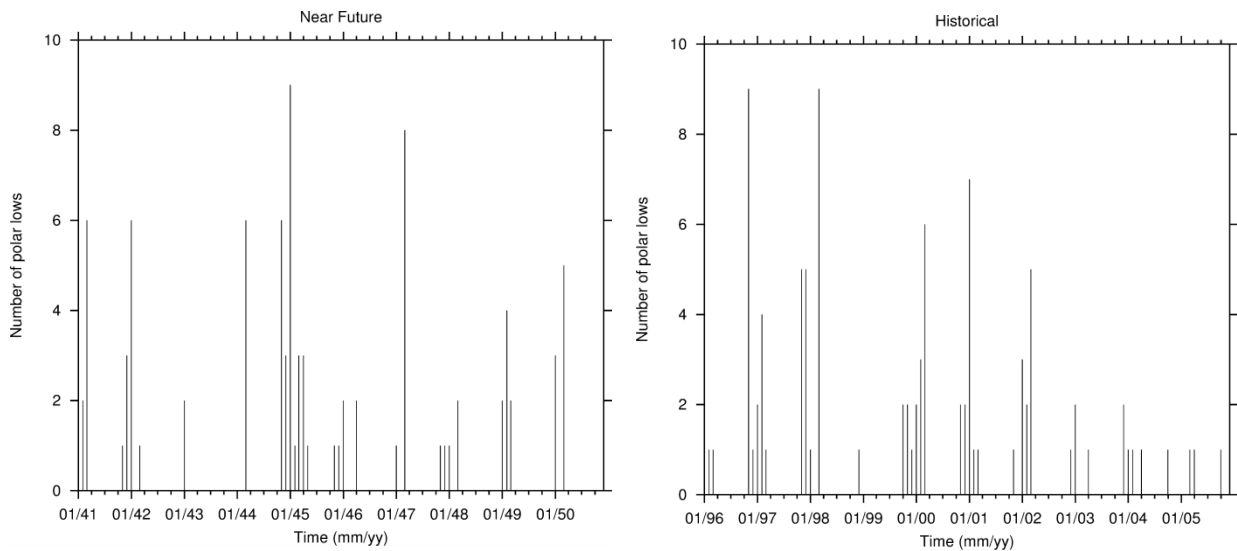
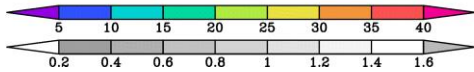
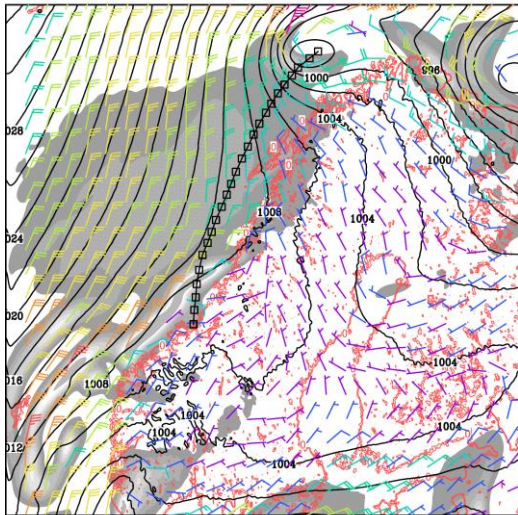


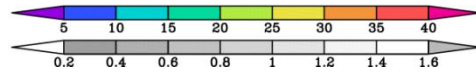
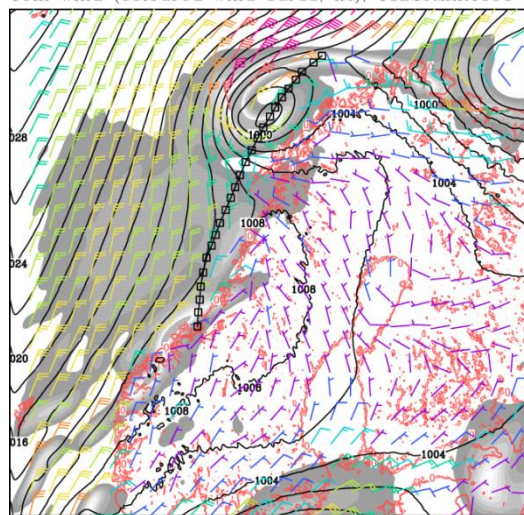
Figure 24: Time series of polar low counts for the historical (left panel) and near future (right panel) simulations.

Fig. 25. shows an intense polar low case. The polar low develops in a cold air outbreak, migrates along a southward track and makes “landfall” in the southern part of Norway. The cyclone also develops rainbands associated with intense precipitation.

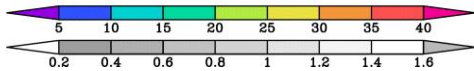
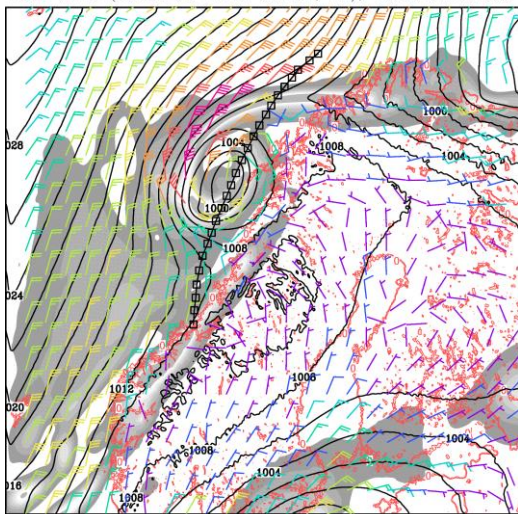
MSLP (contours, hPa), precipitation (shadings, mm/hr), 10m wind (coloured wind barbs, kt), 12Z20MAR1996



MSLP (contours, hPa), precipitation (shadings, mm/hr), 10m wind (coloured wind barbs, kt), 18Z20MAR1996



MSLP (contours, hPa), precipitation (shadings, mm/hr), 10m wind (coloured wind barbs, kt), 00Z21MAR1996



MSLP (contours, hPa), precipitation (shadings, mm/hr), 10m wind (coloured wind barbs, kt), 06Z21MAR1996

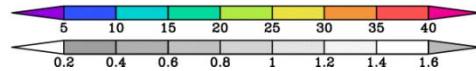
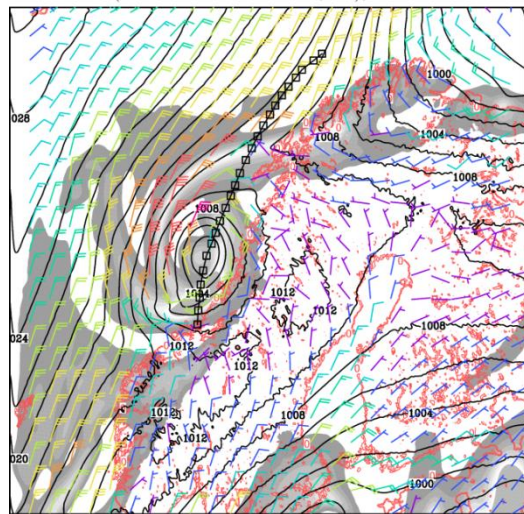


Figure 25: Selected snap-shots of the NEU-3 simulation displaying an intense polar low case (contours: sea level pressure, shadings: precipitation (mm/hr), 10m wind (coloured wind barbs, kts).

Fig. 26 shows polar low frequency versus maximum 10m wind speed. We see that no polar low attains the wind intensity of a hurricane. There is a decrease of extreme maximum wind speed in the near future simulation. Therefore, we cannot see a larger impact by polar lows in the near future on the basis of these simulations.

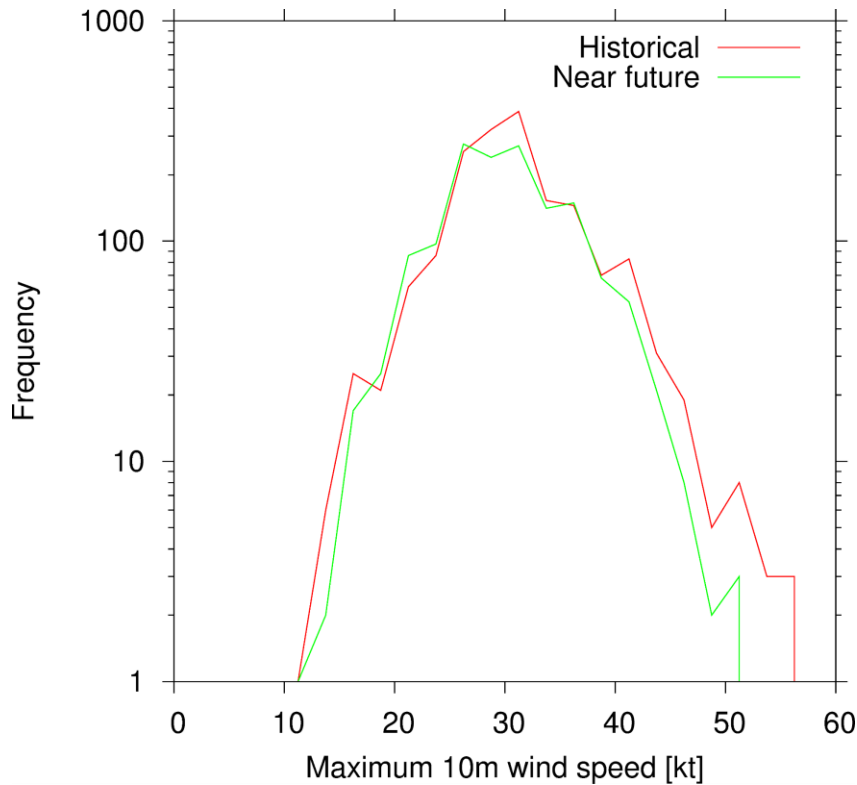


Figure 26: Frequency distribution of maximum 10m wind speed in the polar low identified in the NEU-3 simulations.

#### **4. Lessons learnt and links built**

The report shows that the multi-model based ensemble of CPM simulations provides a basis for manifold studies regarding high impact weather events. On one hand the data formed the input for higher resolved impact models operated within WP4 like the hydrological model wflow\_sbm, the inundation model SFINCS and Global Tide and Surge Model (GTSM) Delft3D FM. On the other hand, direct analysis of CPM simulations also proved to be very beneficial for analysis of high impact weather events in different climates. The rich variety of investigated example events comprises winter storms, continuous heavy rain, droughts, fall Mediterranean heavy precipitation and polar lows. We are optimistic that the data can be applied for further studies. A drawback is that the results of only a few CPM models are available for a specific domain except for the pan-Alpine domain ALP-3. Therefore, one must consider the conclusions with some caution because of the existing scatter of results which can also stem from the driving GCM. On the other hand, for ALP-3 we have a valuable ensemble of many models that can be used for statistically solid investigations on future impacts. Several publications on high impact weather events based on WP3 data are in preparation (e.g. Zander et al., Berthou et al.).

#### **5. References**

Ban, N., Caillaud, C., Coppola, E., Pichelli, E., Sobolowski, S., et al (2021) The first multi-model ensemble of regional climate simulations at kilometer-scale resolution, Part I: Evaluation of precipitation. *Clim Dyn* <https://doi.org/10.1007/s00382-021-05708-w>

Berthou S, Kendon EJ, Chan SC, Ban N, Leutwyler D, Schär C, Fosser G (2020) Pan-european climate at convection-permitting scale: a model intercomparison study. *Clim Dyn* 55:35–59.

<https://doi.org/10.1007/s00382-018-4114-6>

Berthou S., Roberts, M.J., Vanni re B., Belusic D., Caillaud C., Crocker T., Demory M-E, De Vries H. Dobler A, Harris D., Kendon E.J., Landgren O., Manning C. (in prep.) Convection in future winter storms over Northern Europe. *Environmental Research Letters*

Caillaud, C., Somot, S., Alias, A., Bernard-Bouissi res, I., Fumiere, Q., Laurantin, O., Seity, Y., Ducrocq, V. (2021) Modelling Mediterranean heavy precipitation events at climate scale: an object-oriented evaluation of the CNRM-AROME convection-permitting regional climate model. *Clim Dyn* **56**, 1717–1752. <https://doi.org/10.1007/s00382-020-05558-y>

Catto, J. L., Ackerley, D., Booth, J. F., Champion, A. J., Colle, B. A., Pfahl, S., et al. (2019). The Future of Midlatitude Cyclones. *Current Climate Change Reports*, 5(4), 407–420. <https://doi.org/10.1007/s40641-019-00149-4>

Chen, J., Dai, A., Zhang, Y., & Rasmussen, K. L. (2020). Changes in Convective Available Potential Energy and Convective Inhibition under Global Warming. *Journal of Climate*, 33(6), 2025–2050. <https://doi.org/10.1175/JCLI-D-19-0461.1>

Dom nguez, M., Romera, R., S nchez, E., Fita, L., Fern ndez, J., Jim nez-Guerrero, P., ... & Gaertner, M.  . (2013). Present-climate precipitation and temperature extremes over Spain from a set of high resolution RCMs. *Climate research*, 58(2), 149-164.

Deltares, 2019. Delft3D Flexible Mesh Suite. Deltares. <https://www.deltares.nl/en/software/delft3d-flexible-mesh-suite/>

Ducrocq V, Nuissier O, Ricard D, Lebeauvin C, Thouvenin T (2008) A numerical study of three catastrophic precipitating events over southern France. II: Mesoscale triggering and stationarity factors. *Q J R Meteorol Soc* 134(630): 131–145. <https://doi.org/10.1002/qj.199>

Emanuel, K. (2005) Increasing destructiveness of tropical cyclones over the past 30 years. *Nature* **436**, 686–688. <https://doi.org/10.1038/nature03906>

Fumiere, Q., D qu , M., Nuissier, O., Somot, S., Alias, A., Caillaud, C., Laurantin, O., Seity, Y. (2020) Extreme rainfall in Mediterranean France during the fall: added value of the CNRM-AROME convection-permitting regional climate model. *Clim Dyn* **55**, 77–91. <https://doi.org/10.1007/s00382-019-04898-8>

Funk, C., Peterson, P., Landsfeld, M. et al. (2015) The climate hazards infrared precipitation with stations—a new environmental record for monitoring extremes. *Sci Data* **2**, 150066 (2015). <https://doi.org/10.1038/sdata.2015.66>

Grams, C. M., Binder, H., Pfahl, S., Piaget, N., and Wernli, H. (2014) Atmospheric processes triggering the central European floods in June 2013, *Nat. Hazards Earth Syst. Sci.*, 14, 1691–1702, <https://doi.org/10.5194/nhess-14-1691-2014>

Herrera et. al. (2012) Development and Analysis of a 50 year high-resolution daily gridded precipitation dataset over Spain (Spain02). *International Journal of Climatology*, 32:74-85. <https://doi.org/10.1002/joc.2256>

Imhoff, R. O., van Verseveld, W. J., van Osnabrugge, B., & Weerts, A. H. (2020). Scaling point-scale (pedo)transfer functions to seamless large-domain parameter estimates for high-resolution distributed hydrologic modeling: An example for the Rhine River. *Water Resources Research*, 56, e2019WR026807. <https://doi.org/10.1029/2019WR026807>

Kendon, E. J., Roberts, N. M., Fosser, G., Martin, G. M., Lock, A. P., Murphy, J. M., et al. (2020). Greater future U.K. winter precipitation increase in new convection-permitting scenarios. *Journal of Climate*, 33(17), 7303–7318. <https://doi.org/10.1175/JCLI-D-20-0089.1>

Leijnse, T., van Ormondt, M., Nederhoff, K., van Dongeren, A., (2021). Modeling compound flooding in coastal systems using a computationally efficient reduced-physics solver: Including fluvial, pluvial, tidal, wind- and wave-driven processes, *Coastal Engineering*, 163, 10.1016/j.coastaleng.2020.103796.

Manning, C., Kendon, E. J., Fowler, H. J., Roberts, N. M., Berthou, S., Suri, D., & Roberts, M. J. (2021). Extreme windstorms and sting jets in convection-permitting climate simulations over Europe. *Climate Dynamics*. <https://doi.org/10.1007/s00382-021-06011-4>

Mishra, A. K., & Singh, V. P. (2010). A review of drought concepts. *Journal of hydrology*, 391(1-2), 202-216.

Morel C, Senesi S (2002a) A climatology of mesoscale convective systems over Europe using satellite infrared imagery I: Methodology *Quarterly Journal of the Royal Meteorological Society: a journal of the atmospheric sciences. Appl Meteorol Phys Oceanogr* 128(584):1953–1971. <https://doi.org/10.1256/003590002320603485>

Nuissier O, Ducrocq V, Ricard D, Lebeaupin C, Anquetin S (2008) A numerical study of three catastrophic precipitating events over southern France. I: Numerical framework and synoptic ingredients. *Q J R Meteorol Soc* 134(630):111–130. <https://doi.org/10.1002/qj.200>

Nuissier O, Joly B, Joly A, Ducrocq V, Arbogast P (2011) A statistical downscaling to identify the large-scale circulation patterns associated with heavy precipitation events over southern France. *Q J R Meteorol Soc* 137(660):1812–1827. <https://doi.org/10.1002/qj.866>

Pichelli, E., Coppola, E., Sobolowski, S., Ban, N., Giorgi, F., et al (2021) The first multi-model ensemble of regional climate simulations at kilometer-scale resolution part 2: historical and future simulations of precipitation. *Clim Dyn*. <https://doi.org/10.1007/s00382-021-05657-4>

Ricard, D., Ducrocq, V., & Auger, L. (2012). A climatology of the mesoscale environment associated with heavily precipitating events over a northwestern Mediterranean area, *Journal of Applied Meteorology and Climatology*, 51(3), 468-488. <https://doi.org/10.1175/JAMC-D-11-017.1>

SPREAD (Spanish PREcipitation At Daily scale) [Dataset], (2017). <http://hdl.handle.net/10261/141218>

Ullrich, P.A., C.M. Zarzycki, E.E. McClenny, M.C. Pinheiro, A.M. Stansfield and K.A. Reed (2021) TempestExtremes v2.1: A community framework for feature detection, tracking and analysis in large datasets" *Geosci. Model. Dev.* 14, pp. 5023–5048, doi: 10.5194/gmd-14-5023-2021

Van Bebber, W. J. (1891). *Die Wettervorhersage: eine praktische Anleitung zur Wettervorhersage auf Grundlage der Zeitungswetterkarten und Zeitungswetterberichte: für alle Berufsarten.* Enke.

Zahn, M., & von Storch, H. (2008). Tracking polar lows in CLM. *Meteorologische Zeitschrift*, 17(4), 445.  
<https://doi.org/10.1127/0941-2948/2008/0317>

Zander, M.J., Viguurs, P.J., Sperna Weiland, F.C., and Weerts, A.H. (2021): Using convection-permitting climate models and a high-resolution distributed hydrological model to assess future changes in Alpine flash floods., EGU General Assembly 2021, online, 19–30 Apr 2021, EGU21-11484,  
<https://doi.org/10.5194/egusphere-egu21-11484>

Zarzycki, C.M. and P.A. Ullrich (2017) Assessing sensitivities in algorithmic detection of tropical cyclones in climate data *Geophys. Res. Lett.* 44 (2), pp. 1141-1149, doi: 10.1002/2016GL071606